

SEARCH FOR NEW ISOMERS
IN
YTTRIUM, NIOBIUM, ANTIMONY
AND IODINE.

by

Amal C. Ghosh, M.Sc.

A thesis submitted to the Faculty of Graduate Studies and
Research in partial fulfilment of the requirements for the
degree of Doctor of Philosophy.

Department of Physics,
Radiation Laboratory,
McGill University,
Montreal.

April 1961.

SUGGESTED SHORT TITLE:

SEARCH FOR NEW ISOMERS

in

Y, Nb, Sb, I.

Table of Contents.

	Page
I. Introduction.	4
II. General description of the experimental arrangements:	
1. The extraction and focussing system.	6
2. The castle and the detector.	10
3. Monitoring detector and control circuit.	14
4. Energy analysis system.	15
5. Time analysis circuitry.	16
III. Measurements:	
1. Measurement of beam current.	19
2. Energy degradation of the proton beam.	27
3. Resolution, Efficiency and Linearity of the detector.	27
IV. Procedure:	
1. Exploration.	30
2. Measurements:	
a) Half-life.	36
b) Energy spectrum.	36
c) Shape of energy spectrum.	37
d) Yield curve and threshold for the reaction.	38
3. Probable Errors.	39
V. Results:	
1. Yttrium.	40
2. Niobium.	47
3. Antimony.	53
4. Iodine.	64
VI. Summary.	80
VII. Acknowledgements.	81
VIII. Bibliography.	82

List of Figures.

- Fig. 1. Layout of the Extraction and Deflection systems and the Castle.
- Fig. 2. The sector magnet.
- Fig. 3. Diagrammatic representation of the cycle of events.
- Fig. 4. Block diagram of the electronics.
- Fig. 5. Energy spread of protons with degradation in energy.
- Fig. 6. Resolution of the detector for 1.28 Mev γ -ray.
- Fig. 7. Resolution of the detector for 662 kev γ -ray.
- Fig. 8. Resolution vs. Energy of the detector.
- Fig. 9. Efficiency vs. Energy of the detector.
- Fig. 10. Linearity of the kick sorter.
- Fig. 11. Original spectrum from yttrium target.
- Fig. 12. Original spectrum from niobium target.
- Fig. 13. Original spectrum from antimony.
- Fig. 14. Original spectrum from iodine.
- Fig. 15. Original half-life chart.
- Fig. 16. Yield curve for yttrium target.
- Fig. 17. Half-life for yttrium target.
- Fig. 18. Gaussian distribution of 511 kev γ -ray.
- Fig. 18a Gaussian distribution of 511 kev γ -ray.
- Fig. 19a Gaussian distribution of 155 kev γ -ray from yttrium target.
- Fig. 19b Gaussian distribution of 155 kev γ -ray from yttrium.
- Fig. 20. Gaussian distribution of 260 kev γ -ray from yttrium target.
- Fig. 21. Yield curve from niobium target.
- Fig. 22.
- Fig. 23. Half-life from niobium target.
- Fig. 24. Gaussian distribution of 68.4 kev calibration X-ray.

- Fig. 25. 120 keV γ -ray from niobium target.
- Fig. 26. Yield curve for antimony.
- Fig. 27.
- Fig. 28. Half-life of antimony.
- Fig. 29. Gaussian distribution of 662 keV calibration γ -ray.
- Fig. 30. Gaussian distribution of 80 keV γ -ray of antimony.
- Fig. 31. Gaussian distribution of 460 keV γ -ray of antimony.
- Fig. 32. Critical absorption of antimony X-rays.
- Fig. 33. Yield curve for iodine.
- Fig. 34.
- Fig. 35. Half-life of iodine.
- Fig. 36. Gaussian distribution of 32.88 keV calibration X-ray.
- Fig. 36a
- Fig. 37. Gaussian distribution of the composite peak of iodine at 164 keV.
- Fig. 38. Resolved peaks of iodine at 160 and 190 keV.
- Fig. 39. Critical absorption of iodine X-rays.
- Fig. 40. Positions of the four isomers on Weisskopf's chart.
- Fig. 41a Suggested decay scheme for yttrium.
- Fig. 41b Suggested decay scheme for antimony.
- Fig. 41c Suggested decay scheme for iodine.

I. Introduction.

Attention was focussed, in 1949, on the Nuclear Shell Model (12) (14) when it succeeded in correlating diversified experimental facts, rather neatly in some cases, and in making definite predictions, many of which were subsequently verified. The scope and importance of the Theory of the Shell Structure have since increased greatly due to the simplicity of its basic assumptions and flexibility for empiricism. These have resulted in increasing areas of success and consequent remoulding of the theory. The early works of Mayer and Jensen and co-workers have been expanded notably by Bohr and Mottelson, Rainwater, Ford and Wheeler, and others, in explaining the statistical or "liquid drop" properties of nuclei in terms of the single particle model.

One of the early predictions of the Shell Model was that the phenomenon of isomerism should be limited to three broad regions in the periodic table of elements - the so-called "islands" of isomers. Prior to that isomerism was regarded as an accidental phenomenon having equal chances of finding throughout the range of elements. Following the prediction of the Shell Theory, Goldhaber (15) showed that most of the isomers, assigned outside the three islands, actually did not belong there. The present author carried out such an investigation, in 1950, which proved that the isomerism assigned to Ti^{51} was in fact in Ta^{182} occurring in titanium as impurity (16).

The most remarkable feature of the Single Particle Model was the simplicity of its basic assumptions and flexibility for details. Thus without attempting to give the precise order of the levels within a shell it provided the basis for finding out experimentally the actual order of levels in different shells in different nuclei. This information is accumulating and has helped to work out various details of the theory.

The arrangements at the Radiation Laboratory for measuring isomeric states of half-lives between micro-seconds and milli-seconds, using the extracted proton beam, offer an opportunity to study the levels in nuclei. Information on isomers within this range is rather limited.

The present investigation was the result of a plan to search for isomerism in the odd-even nuclei. Out of the eight odd-even elements that were bombarded, four resulted in isomers. This thesis reports the results of these four isomers and of attempts to correlate these results in terms of the Single Particle Model.

II. General Description of the Experimental Arrangements.

The overall experimental apparatus consists of five major parts.

These are:

- 1) Arrangements for extracting the pulsed proton beam from the cyclotron and for focussing the beam by means of a sector magnet on the target.
- 2) The target-scintillation-detector assembly, housed in a castle to shield off unwanted background radiations; and a sink to absorb the residual proton beam.
- 3) The control circuit and the monitoring crystal detector.
- 4) The energy analysis equipment.
- 5) The time analysis circuitry.

1. The Extraction and Focussing System.

The pulsed proton beam, inside the cyclotron, is intercepted by a uranium scatterer, fixed near the periphery of the dee. The position and orientation of the scatterer can be manipulated from outside. The energy of the proton beam is 90 Mev when intercepted. The scattered beam is directed out of the magnetic field through iron channels, which allow the radius of the proton beam to increase rapidly by reducing the magnetic field. Once out of the field of the cyclotron magnet, the divergent beam follows a tangential course to the 44° sector magnet, designed to bend and focus the beam to the target position. The target and the sector magnet are separated by the 11 ft. concrete wall of the cyclotron room. The evacuated pipe, leading the proton beam from the cyclotron to the target, ends in a .005" thick **duural** foil. From this point to the target, the proton beam travels in air a distance of about 2 ft.

During the course of the present investigation some adjustments, rebuilding and addition to the extraction system were necessary.

By taking photographs at various points along the beam path, it was found that the beam cross-section was too large at the target position and that the plane of the proton trajectory and the median plane of the sector magnet was not the same but differed by about one inch. This non-alignment and lack of focussing resulted in a poor beam current.

After proper alignment by raising the sector magnet, a pair of iron wedges was introduced inside the cyclotron chamber near the scattered beam in an attempt to improve the beam current. By adjusting the position of this iron jaw it was possible to increase the beam current considerably.

The next step was to improve the focussing of the beam at the desired point. A series of six photographs, from the sector magnet to the target, were taken to locate the position of the minimum beam cross-section. From this data the optical constants of the sector magnet were recalculated using the equations given by Cross (1). It was found that to have the beam focussed at the target position the entrance and exit angles of the sector magnet faces have to be changed from their existing value. This was done by attaching four additional wedges to the faces. This reduced the beam cross-section at the target from 2" to 1 cm in diameter.

In June 1959 the coils of the sector magnet burnt out. C. K. Hargrove and the writer redesigned it and built together the cooling system. The coils were wound by a commercial firm and the magnet was re-assembled in the Radiation Laboratory. The new coil system was designed for 15% higher current density; and to match this, the cylindrical iron core was expanded by putting in an extra sleeving of iron.

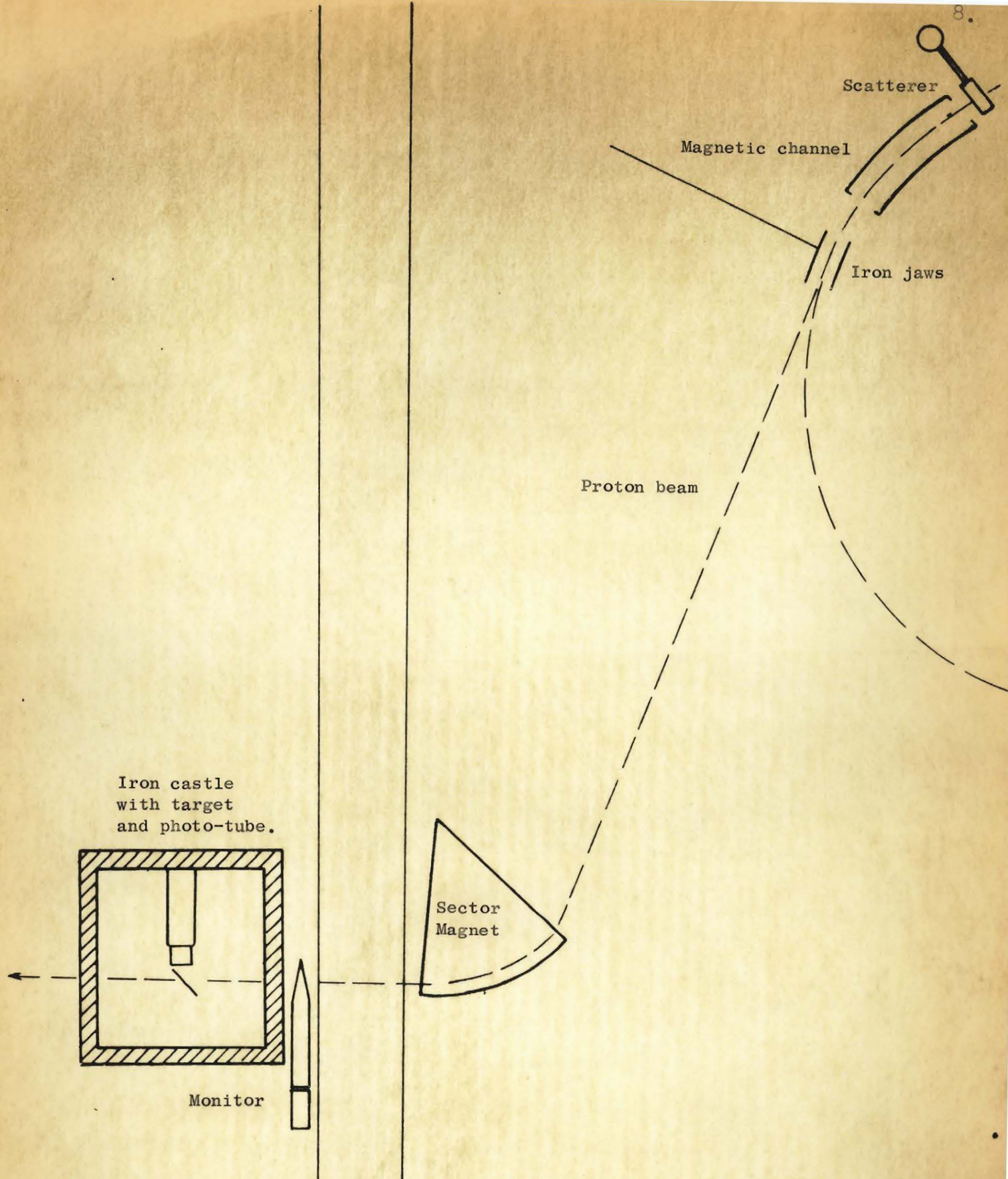


Fig. 1

The layout of the extraction and deflection systems and the castle.

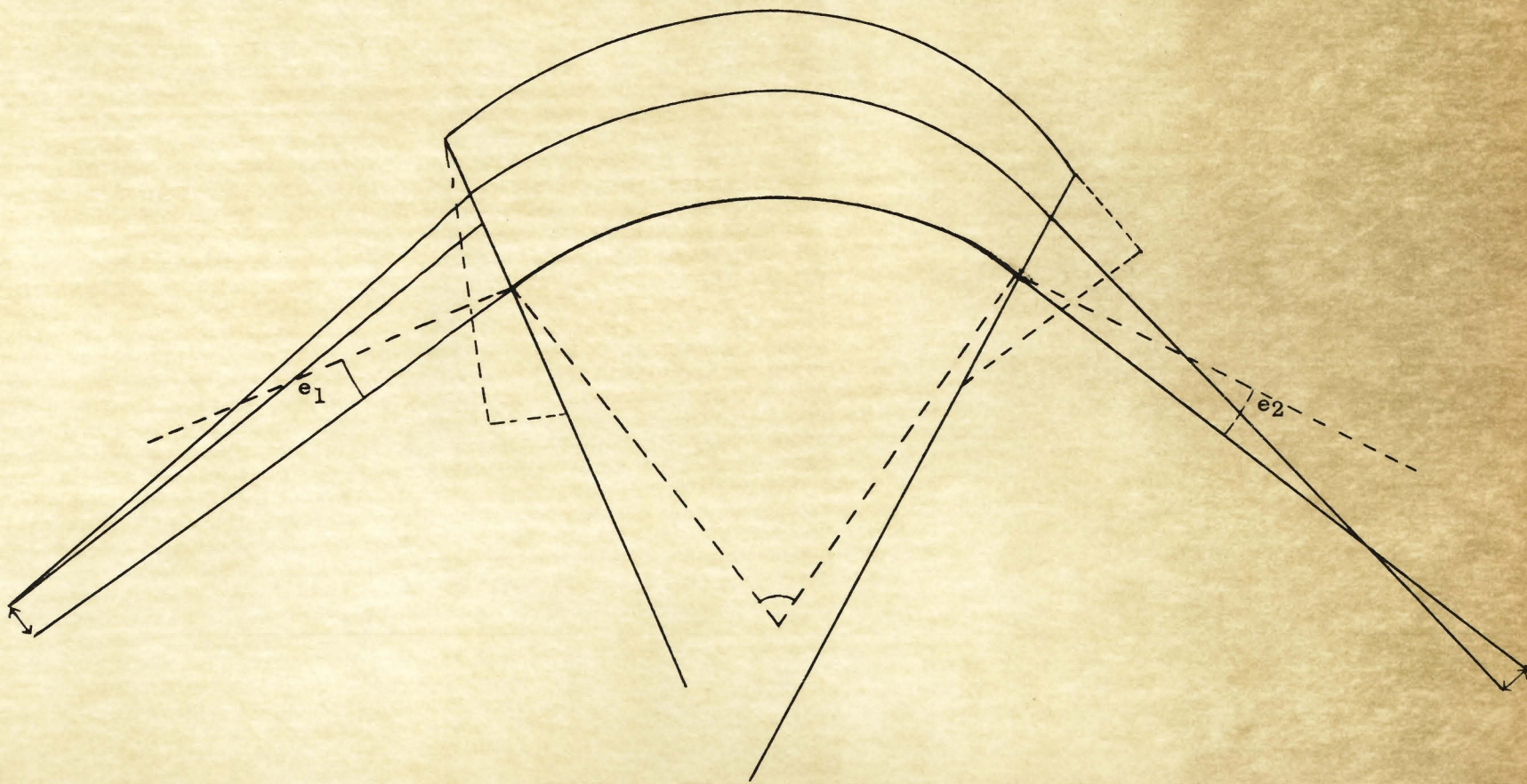


Fig.2. Sector magnet. The wedges added to change e_1 and e_2 are shown.

The maximum beam current was obtained by adjusting separately the scatterer, the iron jaws and the sector magnet current.

The detailed description of the extraction system, and the current stabilizing circuit for the sector magnet, has been given by Hunt (2). The detailed account of the design, specifications and rebuilding of the coils and the cooling system for the sector magnet, is given by C. K. Hargrove (3).

The layout of the extraction system, the castle and the sink is shown in Fig. 1. Fig. 2 illustrates the optical behaviour of the sector magnet.

2. The Castle and the Detector.

The castle, housing the target and the scintillation detector, was built in the corridor leading to the cyclotron room.

In the beginning of the present investigation, the background intensity was so high that it became clear that the signal to noise ratio must be increased by a factor of 10^2 . During this time the castle consisted of a 5' X 4' X 5' sheet metal tank filled with water. The detector was a photo tube with a 5" X 5" NaI crystal at the centre of the tank. The steps taken to increase signal to noise ratio were to build a castle, 18" X 18" X 18" inside clearance, and 5" thick iron wall on all six sides, and to use a 1.5" X 1.5" crystal instead of the 5" X 5" one. Iron was chosen because of its availability and because on proton bombardment no activity was found with half-life within the range of this investigation.

The castle was built with 18" X 5" X 4" iron bars on a trolley which could be moved along a pair of rails up and down the sloping corridor by means of a motor and winch. The proton beam entered through a circular opening in the castle and after passing through the target emerged through a larger opening on the other side of the castle, and from there straight to the sink.

The sink was a 3' X 2' X 4' rectangular hole in the concrete wall. The hole was partially filled with 3' X 2' X 2" slabs of paraffin impregnated with borax.

The background intensity in the corridor had its minimum value nearly at the midpoint between the two walls of the corridor. This was established by removing the castle away and by allowing the beam to traverse the corridor from the end of the vacuum pipe at one wall to the sink on the other side - without any target. The phototube was placed about six inches from the path of the beam and moved along the beam from one wall to the other. The path of the beam through the corridor could be established at any time by attaching a string from a fixed point at the end of the vacuum pipe to another point in the sink. The actual beam was checked from time to time against this reference line by photographing the beam at the end of the vacuum pipe and at the target. The horizontal position of the beam at the target could be varied by about one inch by changing the excitation current in the sector magnet without visible loss of focussing. However, to make the intensity of the beam current over the target area a more sensitive function of the focussing magnet current a limiting diaphragm was placed in the path of the beam about 6' from the target. The beam position was now fixed and the intensity varied as the magnetic current changed.

The target-detector assembly was placed in the castle in such a way that the 1.5" X 1.5" NaI crystal was at the centre of the 18" X 18" castle. No lead shielding was used because of the isomeric state found by Hargrove (3).

The pulses from the photo-tube were taken through a White cathode follower, along a 40 ft coaxial cable to the room where the energy analysis and time analysis were carried out.

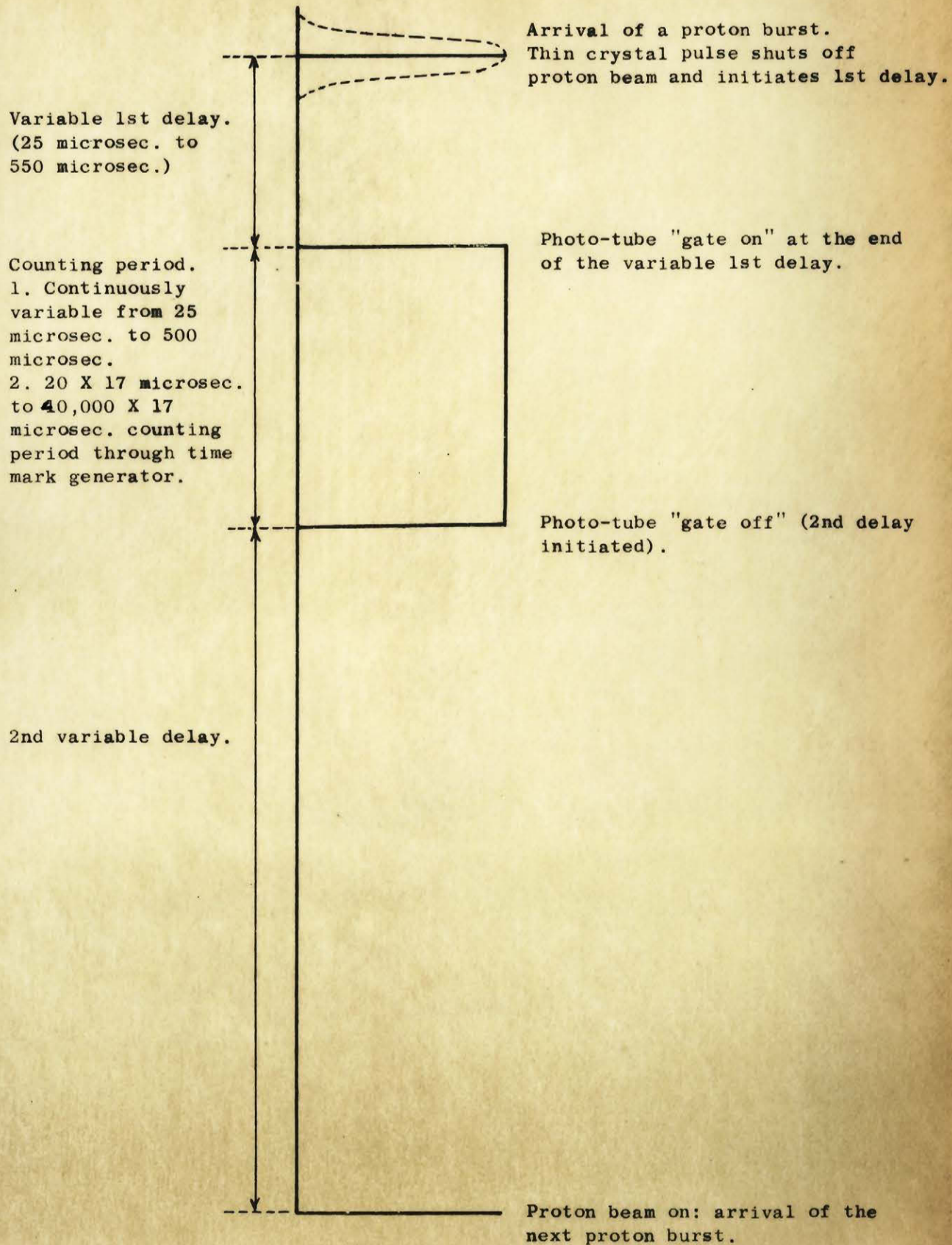


Fig. 3 Diagrammatic representation of the cycle of events.

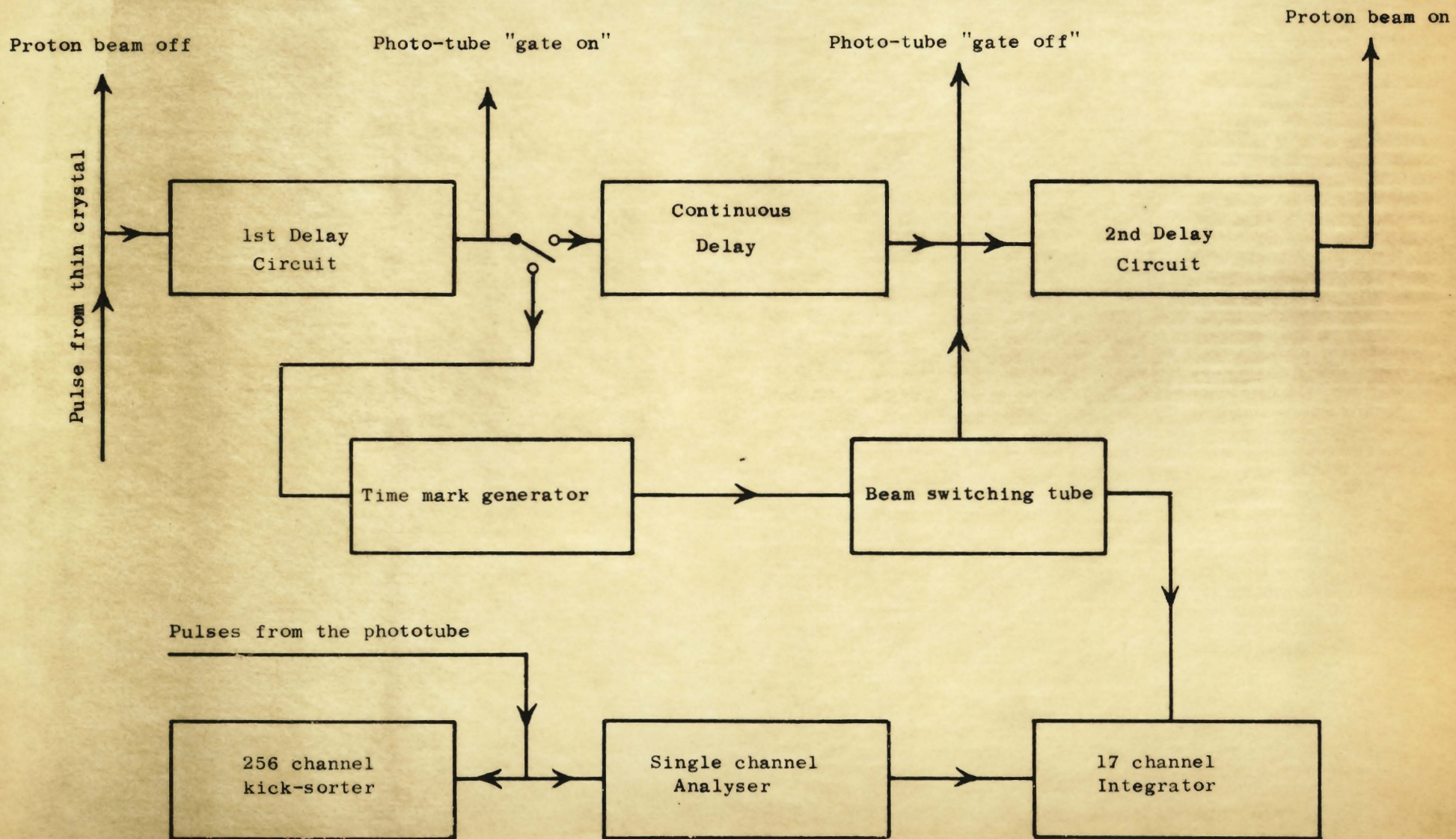


Fig. 4 Block diagram of the electronics.

3. Monitoring Detector and Control Circuit.

A thin phosphor crystal, with 1' long lucite light pipe at the head of a phototube, was used to monitor the beam. The thin crystal was placed just at the end of the vacuum pipe, through which the proton beam emerged. The pulse delivered by the thin crystal phototube assembly went to the control panel through a White cathode follower and 40' of coaxial cable. This monitoring pulse, obtained from each proton pulse in the beam, started the cycle of operations during the interval between two pulses. This cycle is shown on a time scale diagram in Fig. 3.

The width of the proton burst was $\sim 30 \mu$ s. When this burst passed through the thin monitoring crystal it delivered a pulse the height of which was a rough measure of the beam current. This pulse triggered-on the control circuit and at the same time switched off the cyclotron gate. The control circuit consisted of a series of interconnected delay circuits as shown in the block diagram, Fig. 4.

The monitoring pulse was delayed in the control circuit by the first delay circuit which could be varied from 20μ s to 500μ s. At the end of this time the first delay circuit delivered a pulse of about 20 V, which travelled through a coaxial cable back to the phototube in the castle, and neutralized the gate off voltage on the focussing shield of the phototube. The time duration or width of this neutralizing pulse, which determined the gate-on or the counting period, could be varied from 20μ s to $680,000 \mu$ s. At the end of the desired counting period the phototube gate was off and another pulse produced. This pulse actuated a second delay circuit which could be varied from about .0025 sec to 0.1 sec. At the end of this delay the cyclotron gate was opened permitting a second proton burst to be delivered.

thus repeating the cycle. By varying the second delay time the rate of the proton pulse from the cyclotron could be varied from about 10 pulses per second to the full repetition rate of 400/sec of the cyclotron.

The purpose of the 1st delay was to allow the transients associated with the proton burst to die out. The gate-on period determined the total counting interval following each proton pulse. The second delay allowed time for the background to subside before repeating the cycle. The actual values used in a particular case were determined on the basis of the half-life.

The width of each of the pulses introducing the three time intervals were constantly checked on an oscilloscope. The pulses from the thin crystal could be watched on another oscilloscope located at the cyclotron control desk. The pulse height, which was an indication of the proton beam current, was dependent critically upon the tuning of the ion source. The cyclotron was adjusted and tuned by looking at the thin crystal pulse height.

The ammeter and voltmeter registering the current and the voltage applied to the sector magnet were also located on the cyclotron control panel and could be adjusted for maximum beam current, that is maximum pulse height. In general there was no need to adjust the magnet current either during the day or from day to day, due to good stabilization of the current and efficient cooling of the coils.

4. The Energy Analysis System.

The energy analysis system was a 256 channel kick sorter with analogue and digital read-outs. An auxiliary linear amplifier was used for wider gain control. Before each measurement, which generally lasted for about two hours, the kick sorter was calibrated using a reference γ or X-ray line of suitable energy. The calibration γ -rays were 662 keV line from cesium (Cs^{137}) and the 511 keV and 1.28 keV lines of sodium (Na^{22}). The X-rays used were 68.4 keV line

of platinum from gold (Au) and 32.88 keV line of barium from cesium (Cs^{137}). (6)

During the interval that the phototube inside the castle was gated on, the γ -rays from an excited isomeric state were absorbed in the NaI crystal, and the output pulses from the phototube sent to the kick sorter through a White cathode follower and about 50 ft of coaxial cable. In the kick sorter room the pulses from the coaxial line were fed to another White cathode follower. The output pulses from this were fed to the linear amplifier of the kick sorter and, through a single channel analyser, to the time analysis circuit. In the energy spectrum sufficient number of pulses were accumulated under a peak to give acceptable statistical accuracy. By varying the gain of the linear amplifier the energy range could be spread over the desired number of channels. The shape of each energy spectrum was pen-recorded and the corresponding digital readout gave the number of counts in each channel. From these, the intensity, shape and energy of each peak were computed. Four energy spectra are shown in Figures 11 to 14.

5. Time Analysis.

The time analysis circuit and the control circuit were housed on the same rack in the kick sorter room. These consisted of a seventeen channel integrator, each channel of which could accumulate 1000 pulses. These channels were depicted on a CRT screen on which continuous accumulation of pulses in each channel could be seen. The CRT pattern could be pen recorded for subsequent numerical analysis.

The pulses from the phototube were passed through a single channel analyser, so that pulses corresponding to each of the lines in the energy spectrum could be analysed for half-life separately, whenever necessary. After a line in the energy spectrum had been definitely associated with the measured half-life, the single channel bias was generally adjusted to cut off

scattered γ -rays of lower energy than the line. This kept the background satisfactorily low.

A beam switching tube, operated by a time marker generator, was employed to direct the pulses from one channel to another after a preset time interval. Thus each of the seventeen channels received pulses for a definite interval, one after another; and due to the decay of the excited state the number of pulses accumulated in each channel for the same time would decrease exponentially.

The range of time interval per channel was $20\ \mu\text{s}$ to $40,000\ \mu\text{s}$ in steps of $40\ \mu\text{s}$, $100\ \mu\text{s}$, $200\ \mu\text{s}$, $400\ \mu\text{s}$, $1000\ \mu\text{s}$, $2000\ \mu\text{s}$, $4000\ \mu\text{s}$ and $10,000\ \mu\text{s}$, $20,000\ \mu\text{s}$ to the maximum of $40,000\ \mu\text{s}$. Thus the total counting interval for the phototube would be the interval per channel X the number of channels, namely 17. The shortest counting interval for time analysis was therefore $20 \times 17 = 340\ \mu\text{s}$. However, by a separate time delay circuit, which by-passed the time marker generator, the counting interval could be continuously changed from a minimum of $25\ \mu\text{s}$ to about $250\ \mu\text{s}$. This shorter counting interval was used to get cleaner and better resolved peaks for short-lived γ -rays, by suppressing the pulses from longer-lived background.

The zero-level and the integrated pulse height in each channel could be easily adjusted by varying respectively a resistance and a capacitance in each channel. These channels were regularly adjusted and calibrated with pulses from a precision mercury pulser. After adjusting the zero level each channel was fed with 680 pulses from the pulser. By adjusting the capacitance of each channel the pulse heights for each were made equal. The voltage on the pen recorder was then adjusted so that the pen deflection on the chart corresponded to this number on the chart. Thus, the pen record gave directly the number of γ -rays from the excited state as a function of time in 17 steps

from which the half-life can be obtained directly. The distribution of background counts in the 17 channels were recorded simply by removing the target from the path of the beam. In order to include, however, the scattering effect of the target material towards background an equivalent thickness of copper foil was frequently used in the path of the beam for background measurement. Copper was quite suitable for use as a pure scatterer. No trace of any activity was found in copper within the time range concerned in these experiments, for the entire range of proton energy. A typical half-life and the corresponding background recordings are shown in Fig. 15.

The time analysis and control circuitry are more fully described by Hargrove (3). Integrators are copies of those in the 28 channel kick sorter designed by R. E. Bell. (8)

III. Measurements.

1. Measurement of Beam Current

The beam current was constantly monitored by noting the pulse height from the thin crystal on an oscilloscope. This was used as a check during each run. Whenever necessary the beam current was measured by means of a Faraday cup. During such a measurement, the castle, with the target and phototube assembly, was wheeled down the further end of the corridor; and the thin crystal removed. After the proper adjustment of the uranium scatterer, the sector magnet faces, the alignment and the introduction of the iron jaws, the maximum value of the beam current obtained rose to 3.4×10^{-11} amp.

The readings of the Faraday cup were checked ~~for~~ several times in the course of this experiment by measuring the activity induced in a graphite target by the proton beam. A rectangular piece of graphite was fixed at the end of the vacuum pipe by means of scotch tape and bombarded for five minutes at the full pulse repetition frequency. After bombardment the graphite plate was placed in between two aluminium plates to cut off positrons and the intensity of the 511 kev line measured in the kick sorter at intervals ranging from 2 minutes to 5 minutes for about 70 minutes. From this the half-life was plotted and the value of the counting rate at the five minute point extrapolated. The beam current was calculated from the relation:

$$i = \frac{e A}{N_0 \sigma} \frac{1}{pt(1 - e^{-\lambda t})} \cdot \frac{dN}{dt} .$$

From the extrapolated value of dN/dt and the known values of the other quantities, i can be computed. During measurements of the yields of the activities reported here the beam current was measured to be 2.5×10^{-11} amp by the Faraday cup; and the corresponding value from the carbon excitation (C^{11}) data was 2.4×10^{-11} amp.

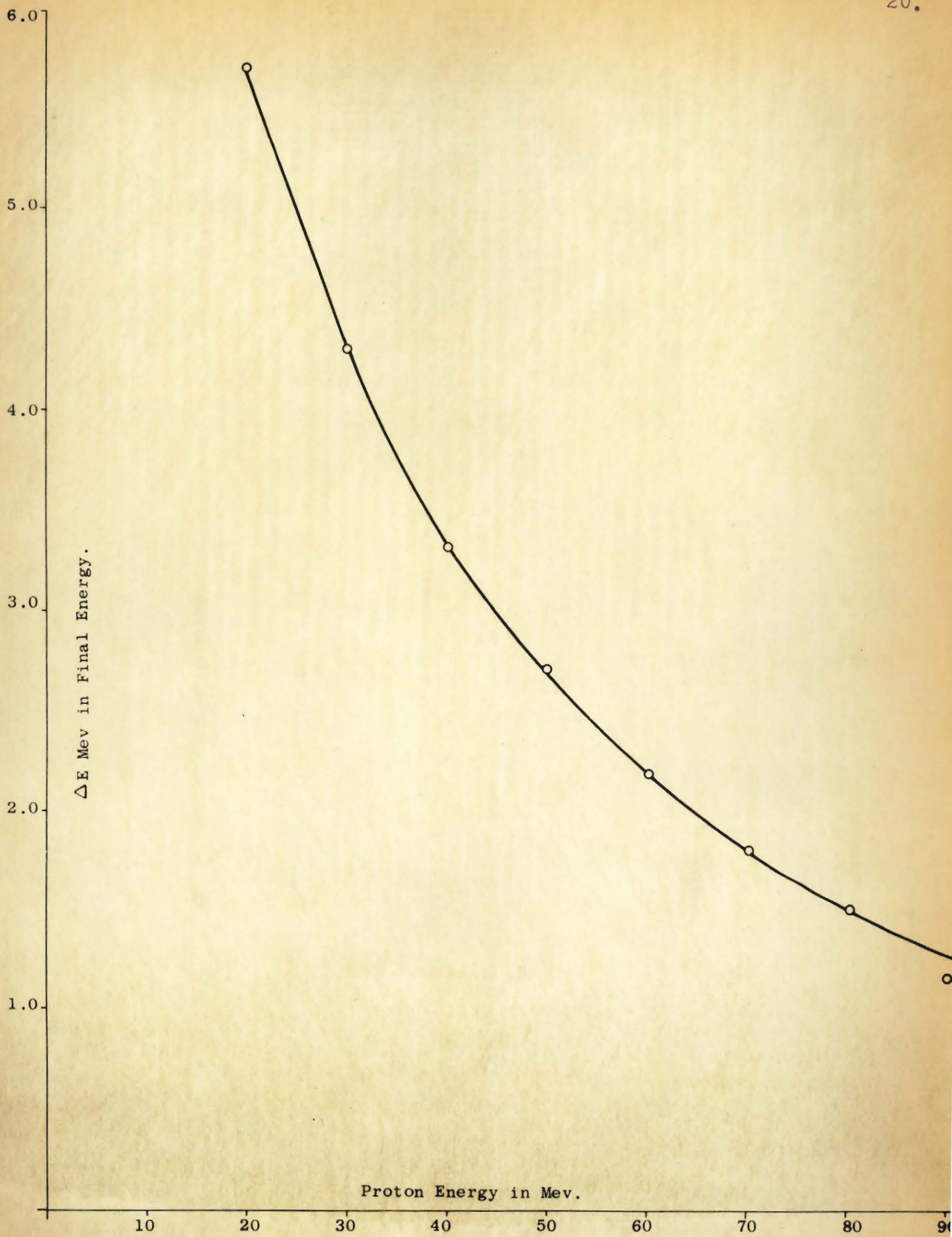


Fig. 5

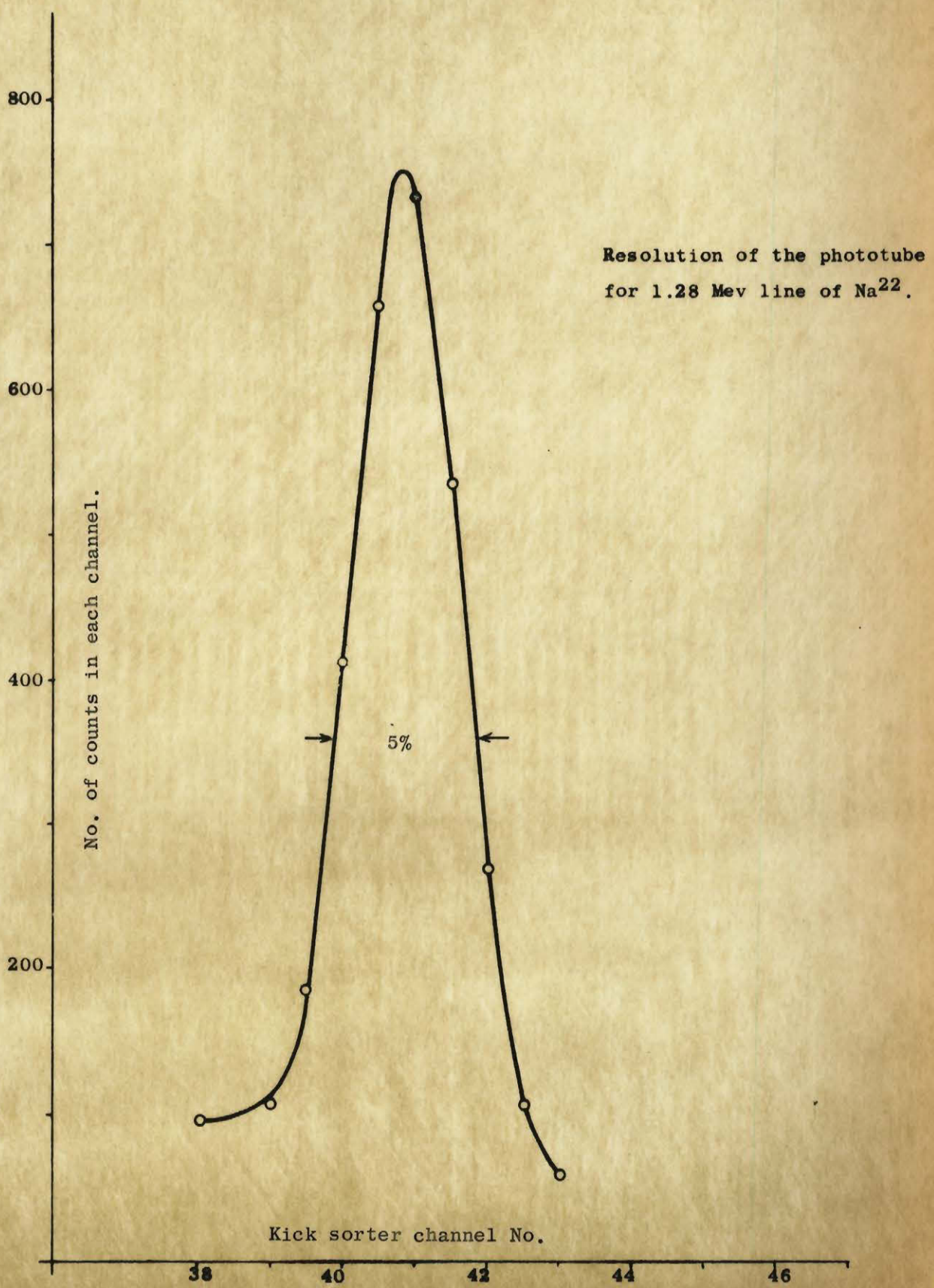


Fig. 6

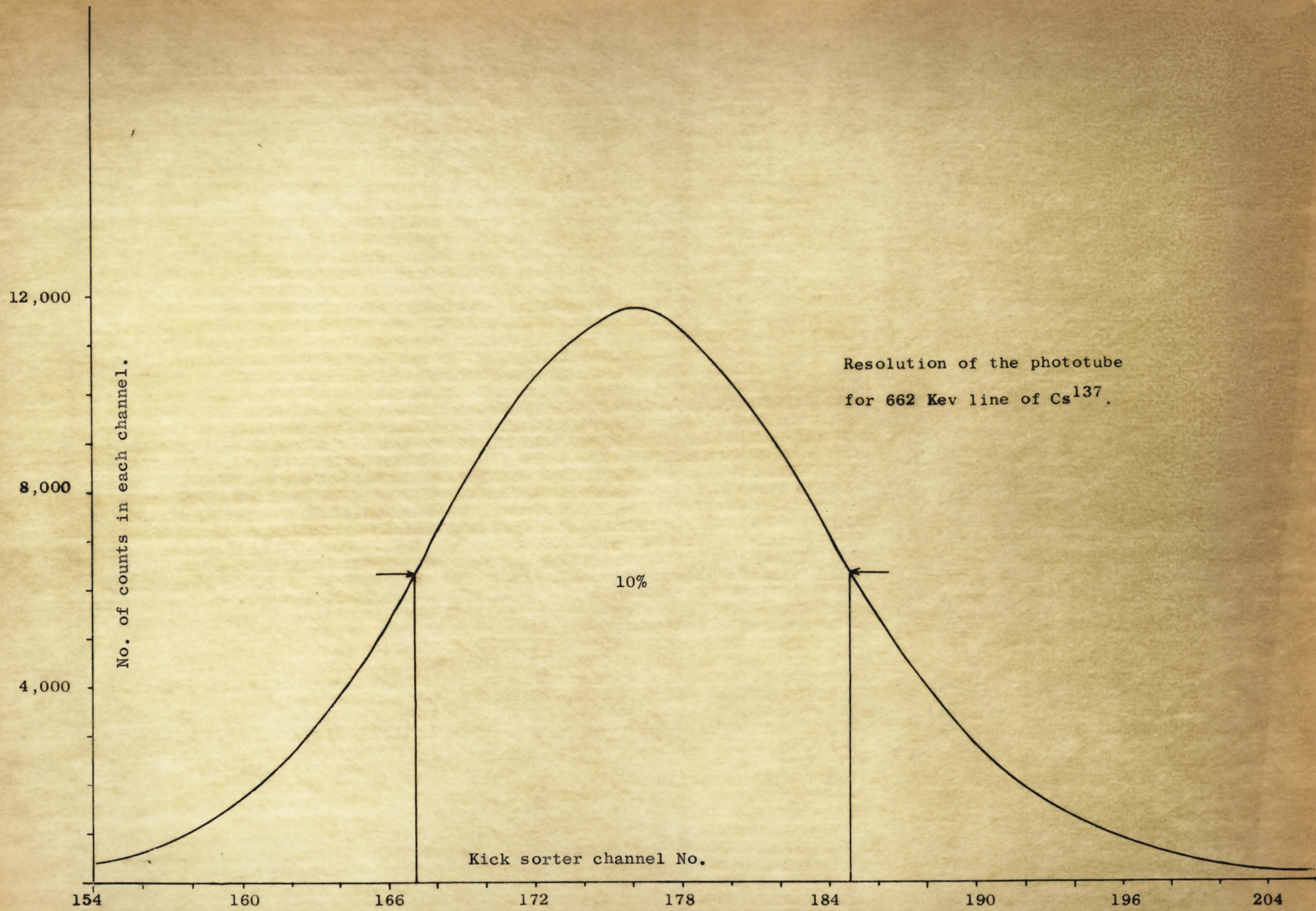


Fig. 7

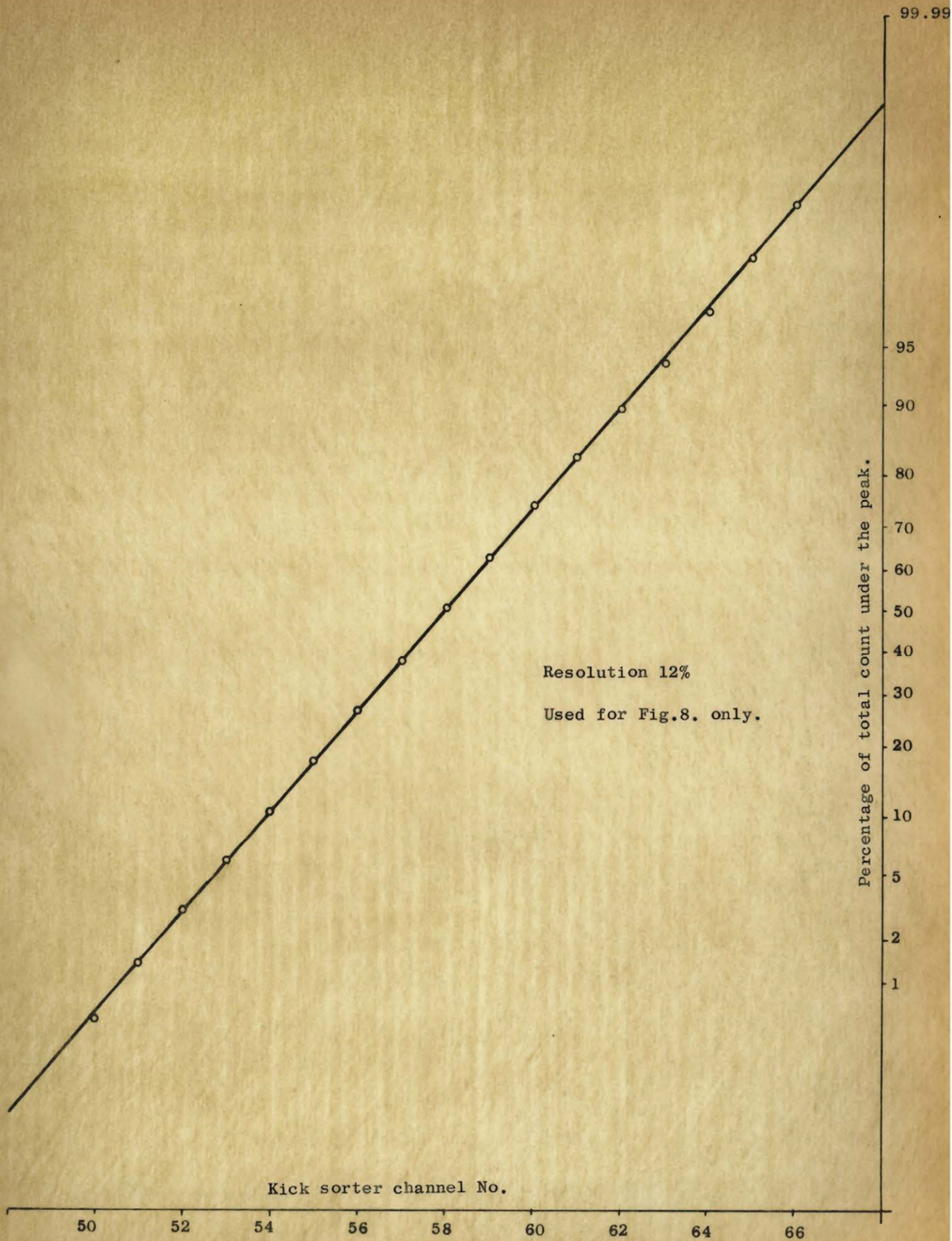


Fig. 18A Gaussian distribution of 511 keV line of Na^{22} .

155 kev
Resolution 40%
Used for Fig. 8. only.

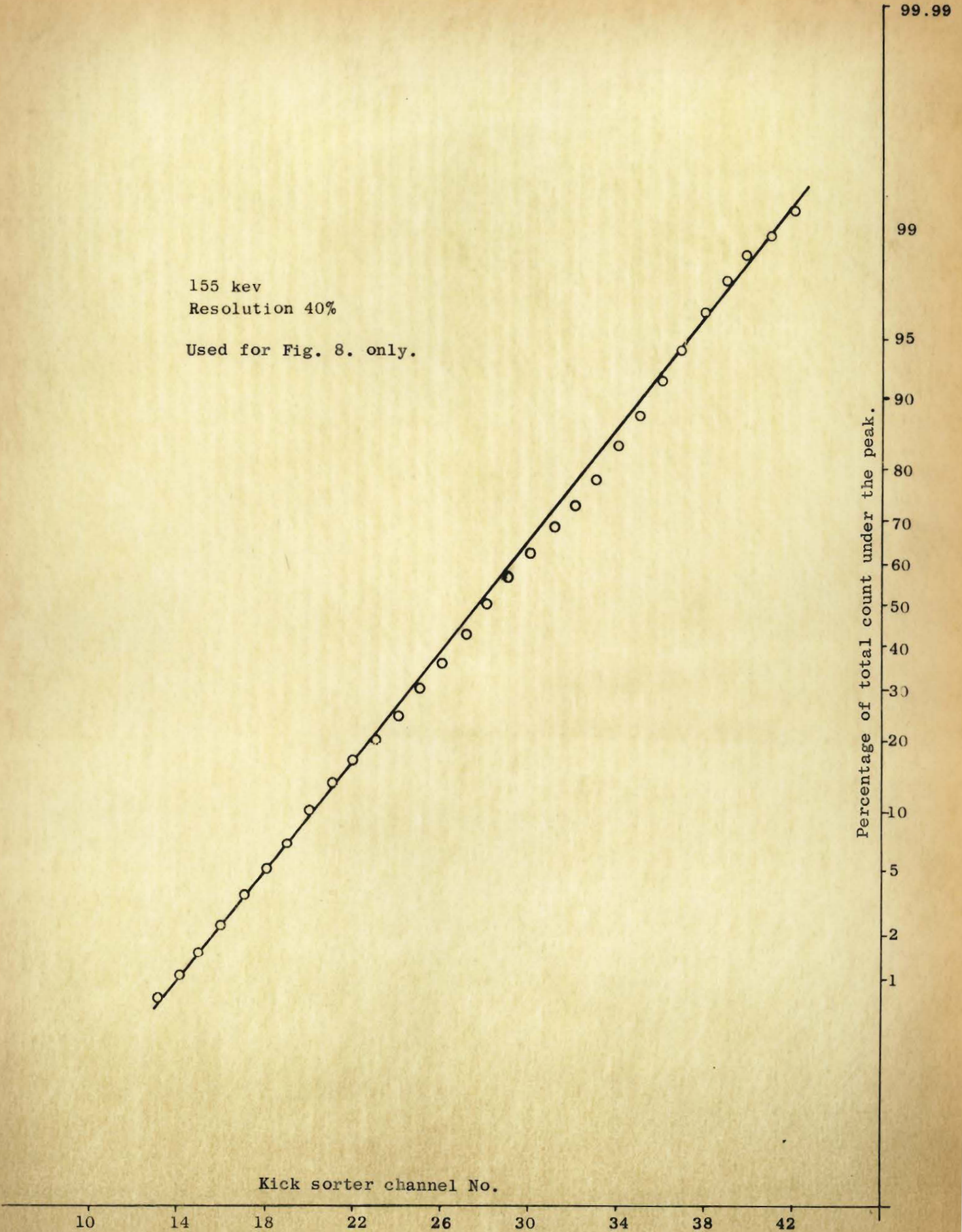


Fig. 19B Gaussian distribution of 155 kev line of Yttrium target.

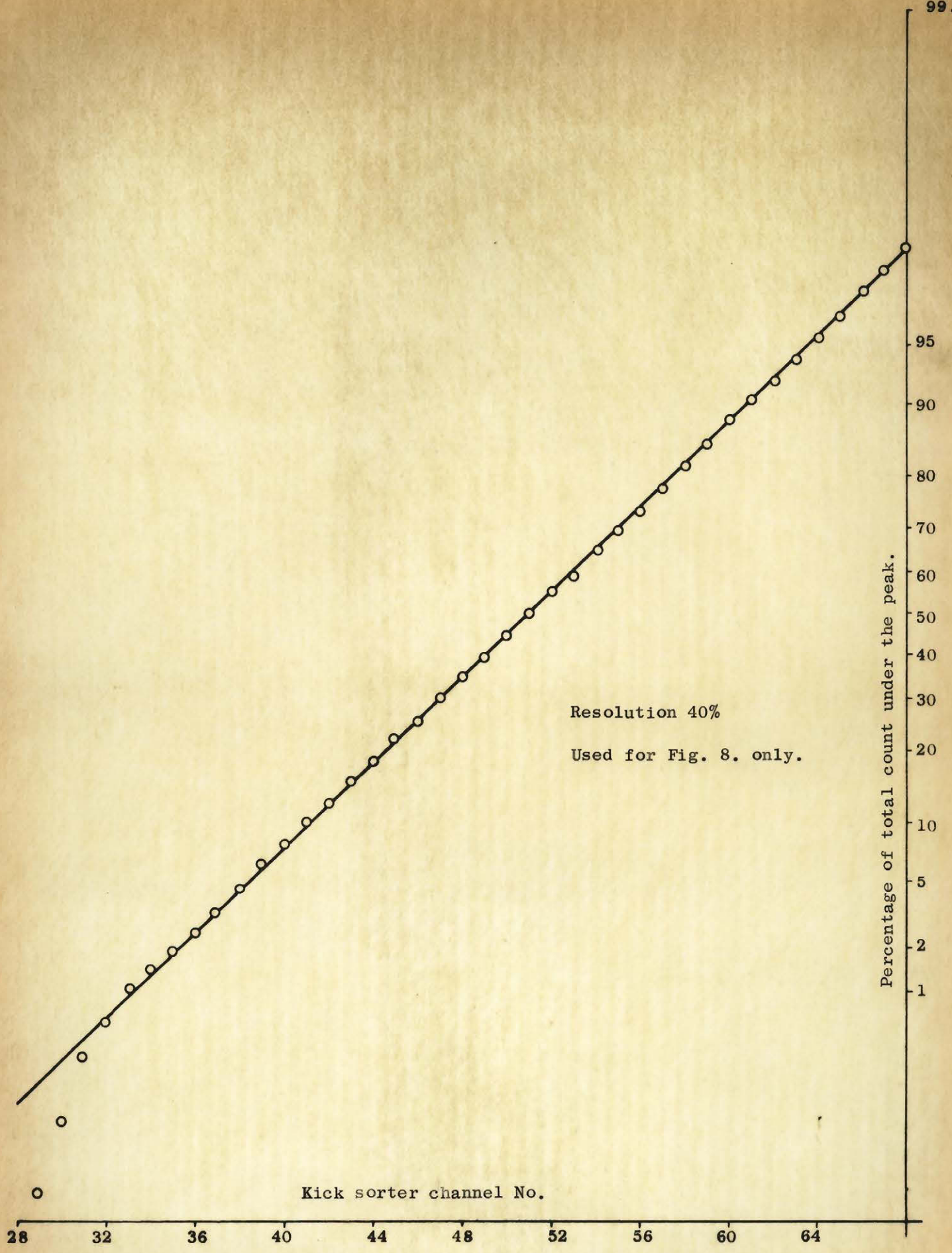


Fig. 36A Gaussian distribution of 32.88 keV calibration line.

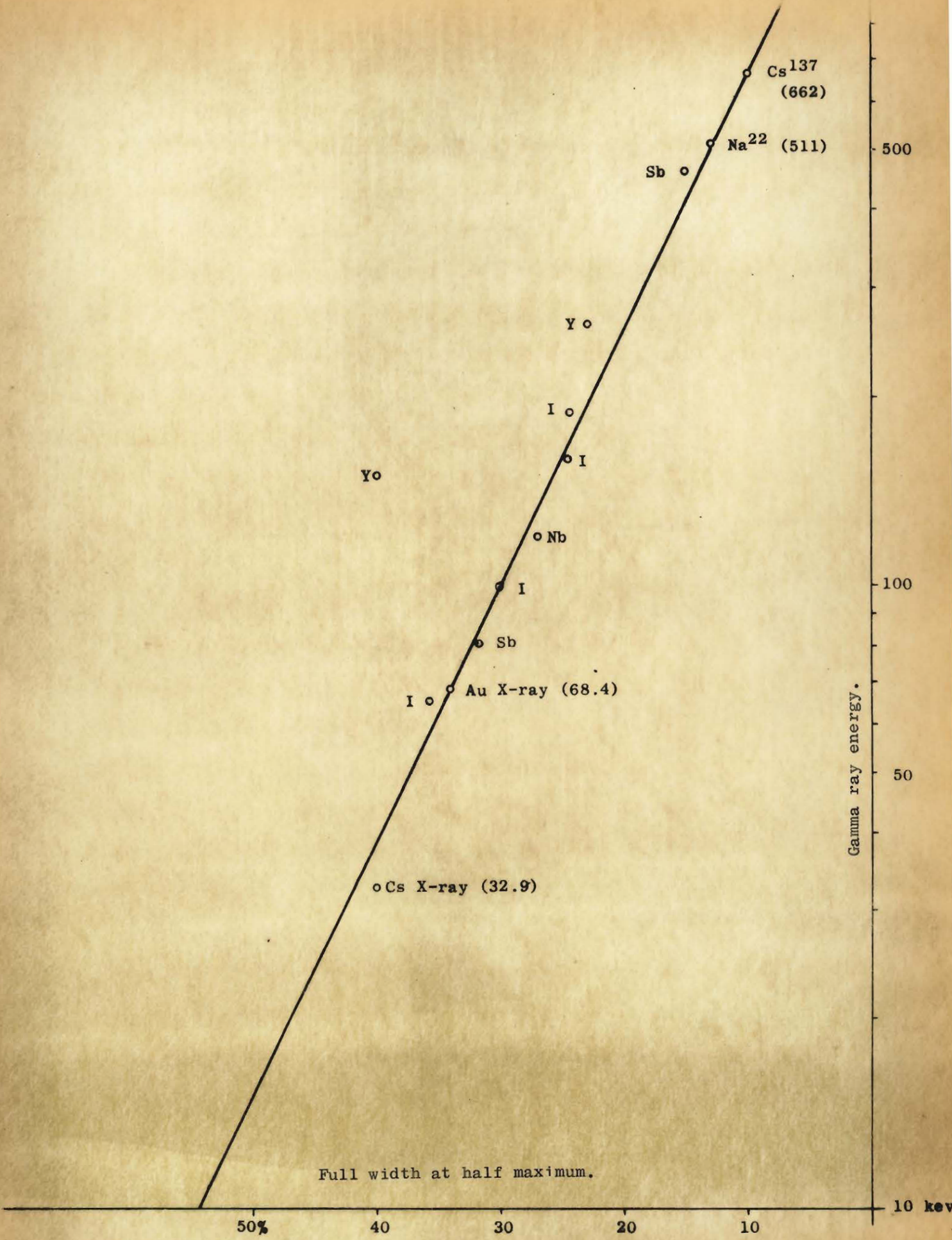


Fig. 8 Energy-Resolution Graph.

2. Energy Degradation of the Proton Beam.

The optical parameters of the sector magnet were adjusted for deflecting and focussing of 90 Mev protons to the target. The full width at half-maximum for the energy spread at 90 Mev was 1.17 Mev (4).

The method used for reducing beam-energy was to interpose graphite absorbers in the path of the beam between the end of the vacuum pipe and the target. A set of eight graphite absorbers were made to decrease the energy from 90 Mev to 10 Mev in steps of 10 Mev. The absorbers were cylindrical with about 2" in diameter and these were usually placed in the hole of the iron castle through which the beam entered. The scattered beam was thus somewhat collimated. The spread in energy for these energies is given in Fig. 5 (4).

3. Resolution, Efficiency and Linearity of the Detector.

The resolution of the phototube was measured for the three γ -rays and two X-rays used as calibration lines throughout this investigation. These lines and their resolutions are tabulated in Table I^{p.77.} The full width at half maximum for the 1.28 Mev line of Na²² and the 662 kev line of Cs¹³⁷ are shown in Figures 6 and 7. The resolution vs energy curve is plotted in Fig. 8. These values have been computed from the Gaussian distribution of the counts under each peak.

The efficiency of the detector for different energies was calibrated against the efficiency of the standard phototube in the kick sorter room (5). The efficiency curves for both are shown in Fig. 9.

The linearity of the phototube electronics and the zero setting of the kick sorter were checked by means of a precision pulser and are shown in Fig. 10.

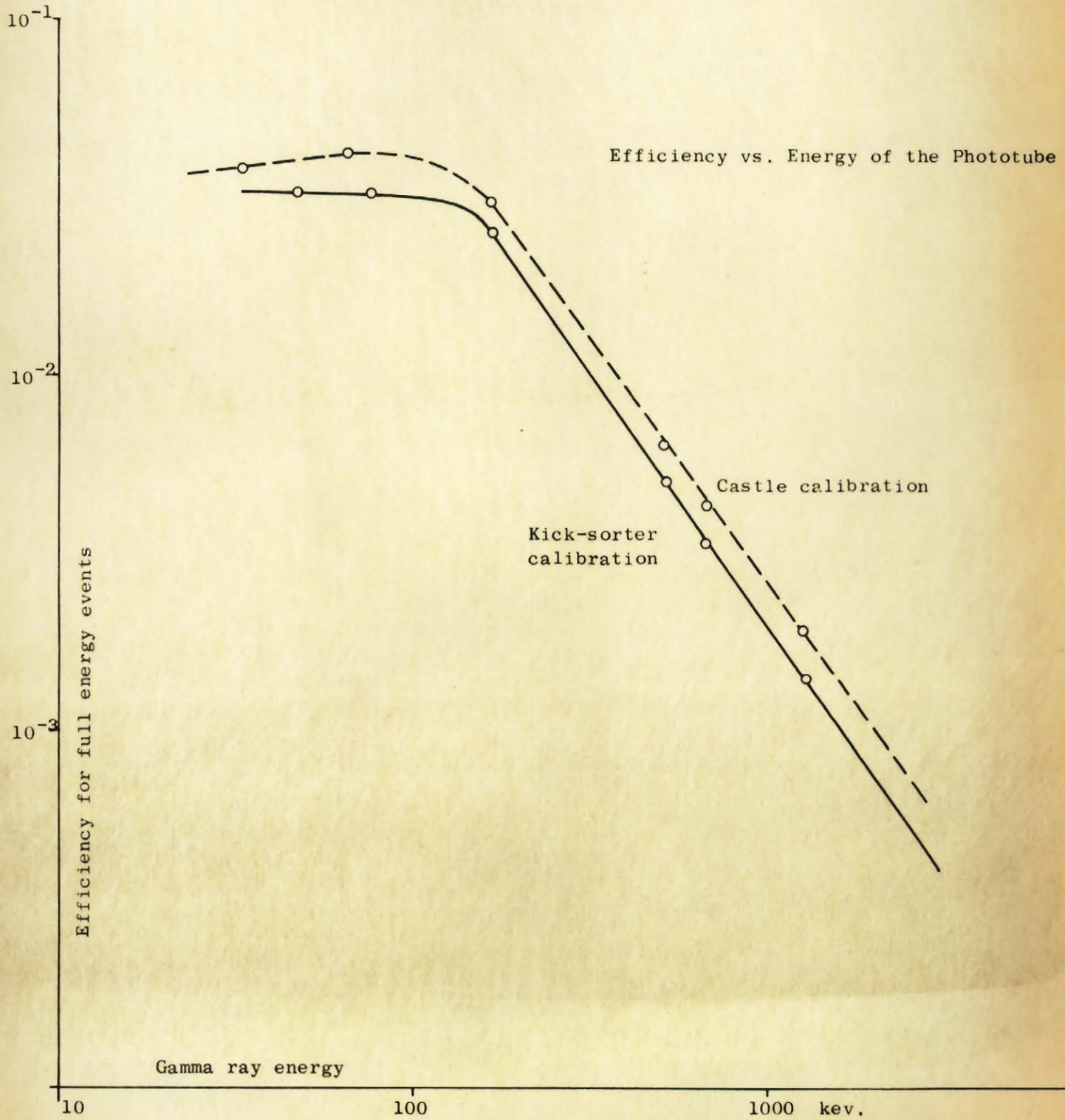


Fig. 9

Linearity of the kick-sorter channels.

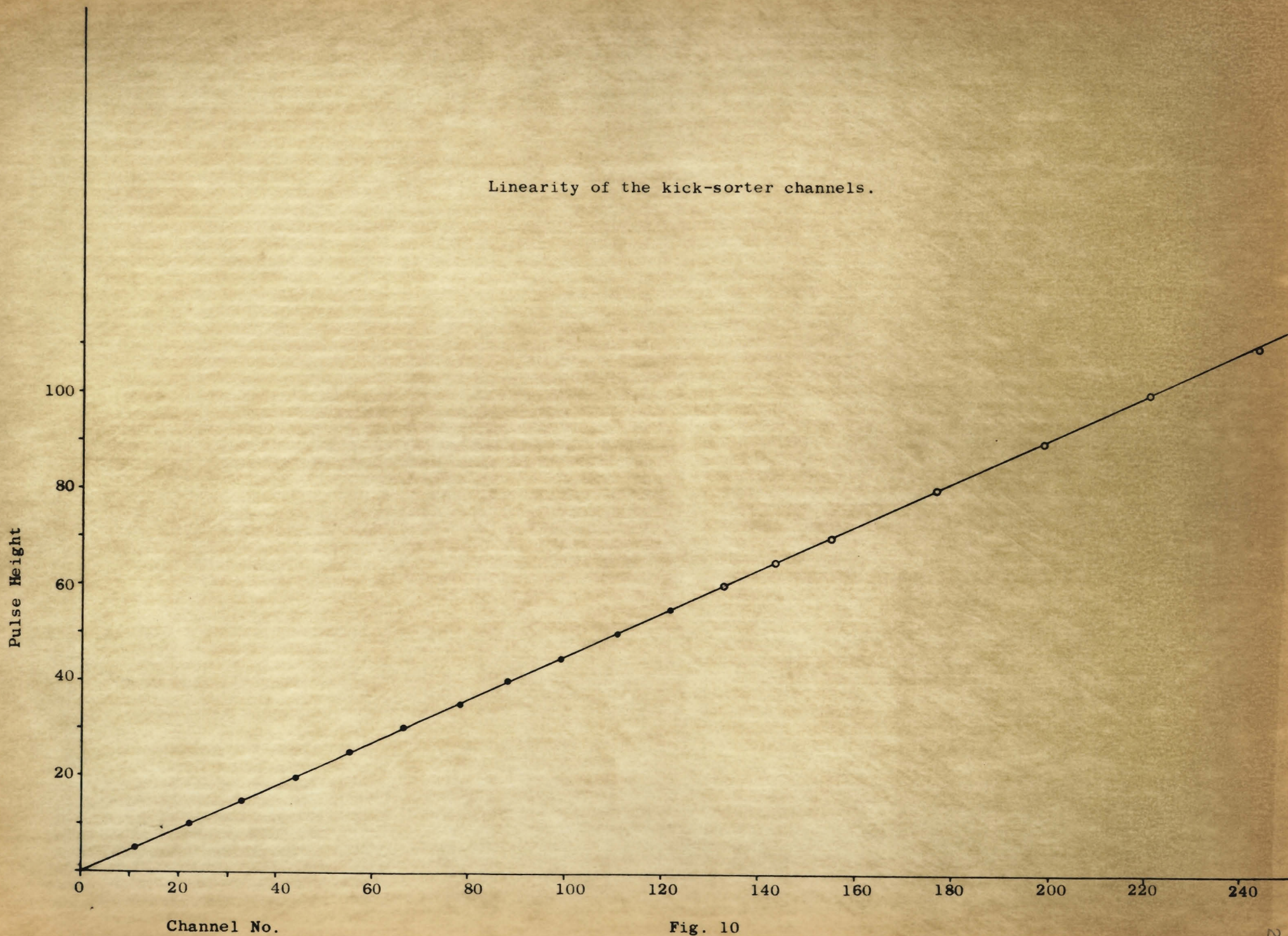


Fig. 10

IV. Procedure.

1. Exploration.

For initial survey rather thick samples were used. When an isomeric state was obtained its energy spectrum was recorded and simultaneously its half-life was measured. During each initial survey a rather high proton pulse rate was used. The area of the targets was about $1.5 \times 2.0 \text{ cm}^2$; and these were fixed on thin cardboard frames, which could be slid into the target holder. Three target holders of brass, aluminium and polystyrene, were used. When an isomeric state was observed for any sample, targets of known dimensions were prepared for further work. Targets were in the form of thin foils, if available, otherwise they were prepared out of finely divided powder.

To start with, a sample would be bombarded with 90 Mev protons and the pulses from the phototube would be simultaneously fed to the kick sorter and the integrator. Starting with $40 \mu\text{s}$ ^{per channel} interval the accumulation of pulses in the 17 channels would be watched. During such a survey run only the lower level bias of the single channel analyser would be used, and this would be set at about 30 kev. If there appeared to be no trace of any definite activity, the search would continue for channel intervals respectively of $100 \mu\text{s}$, $1000 \mu\text{s}$ and $10,000 \mu\text{s}$. In most cases any half-life within the range of this equipment could be traced by using these four broad ranges; and once the order of magnitude of the half-life was known, a suitable time range was chosen for final measurement. If no activity could be detected for the whole range of the time scale for 90 Mev proton bombardment, then the beam energy would be reduced by 10 Mev steps and the search would be repeated for each energy.

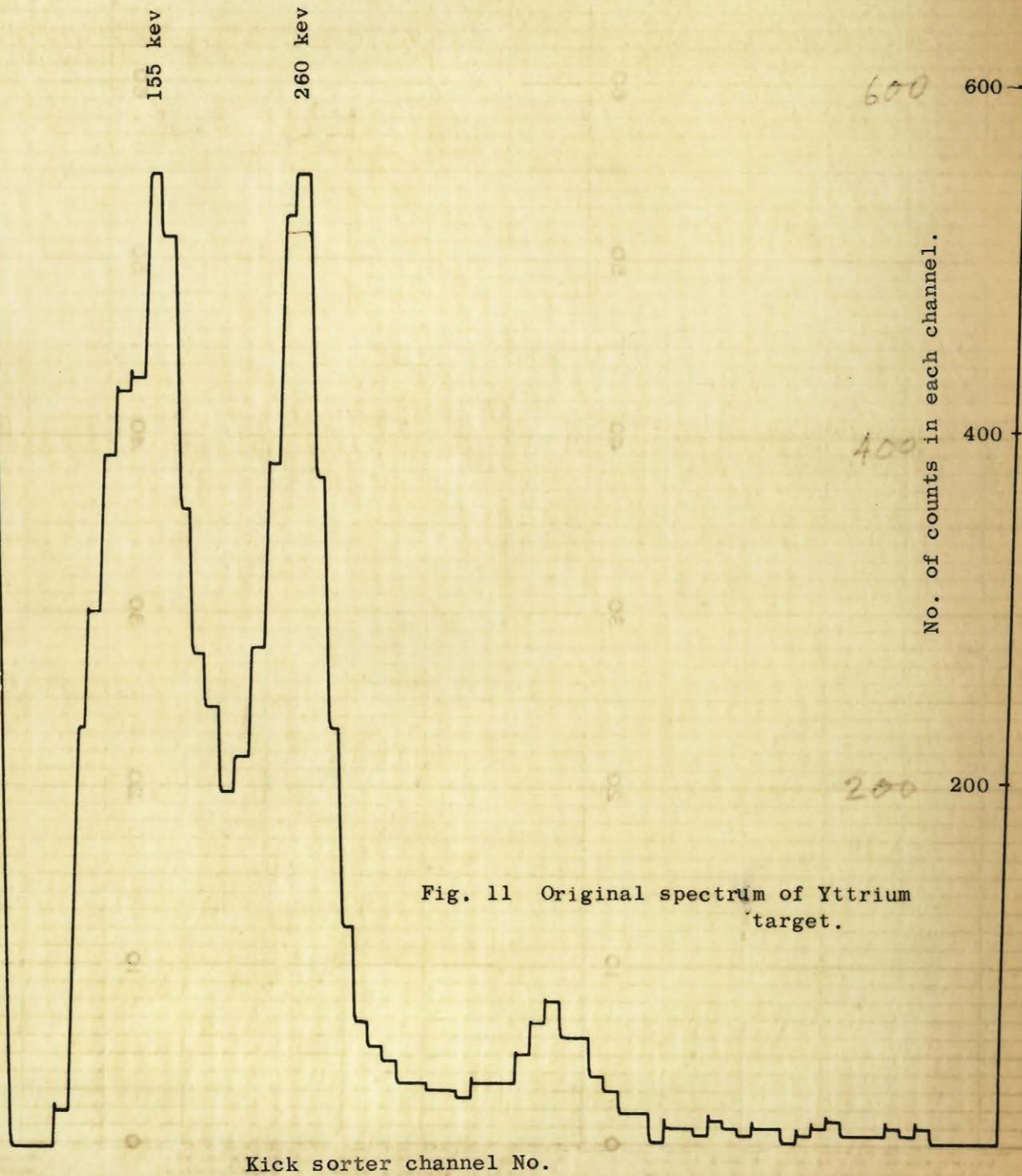


Fig. 11 Original spectrum of Yttrium target.

Kick sorter channel No.

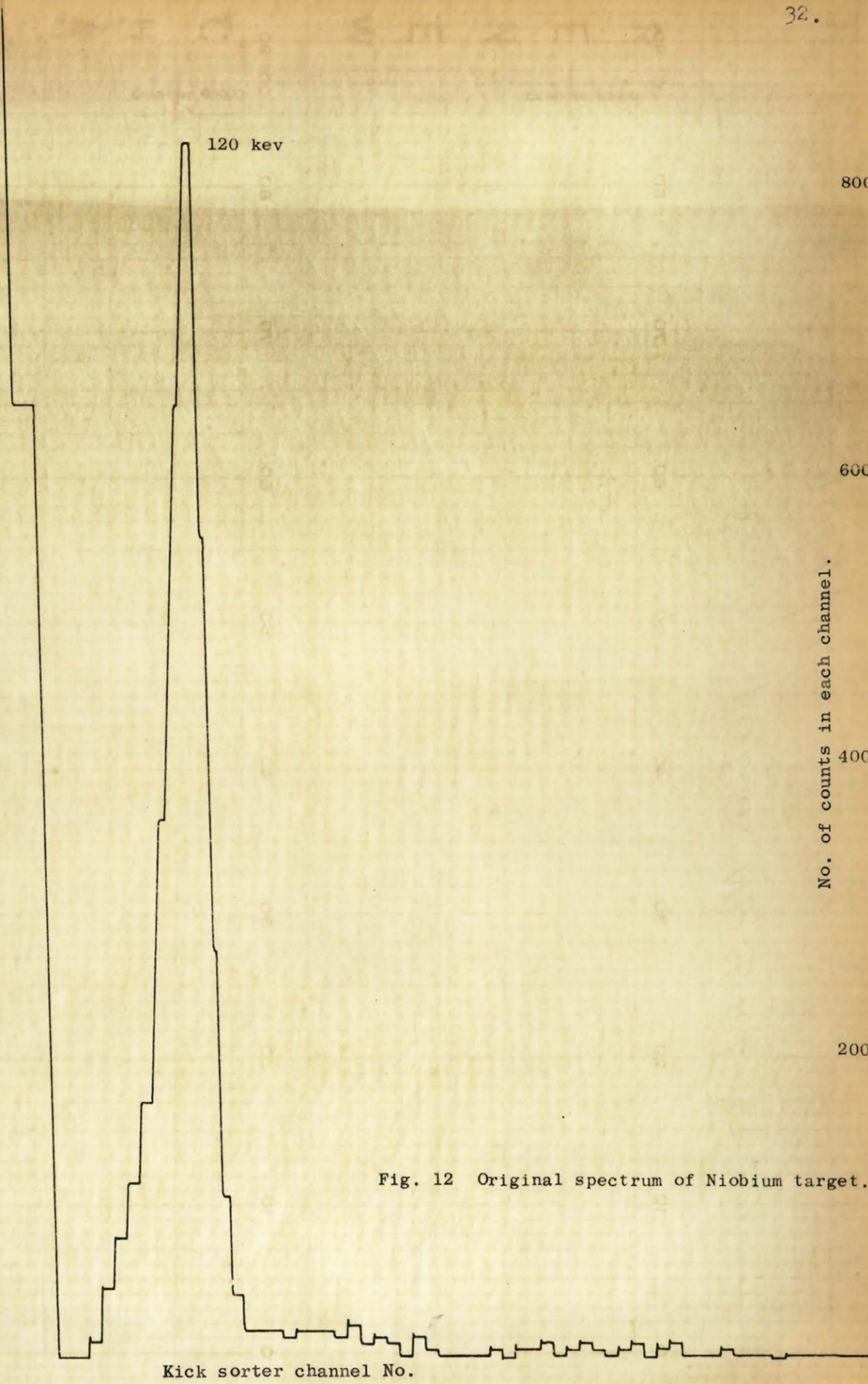


Fig. 12 Original spectrum of Niobium target.

Kick sorter channel No.

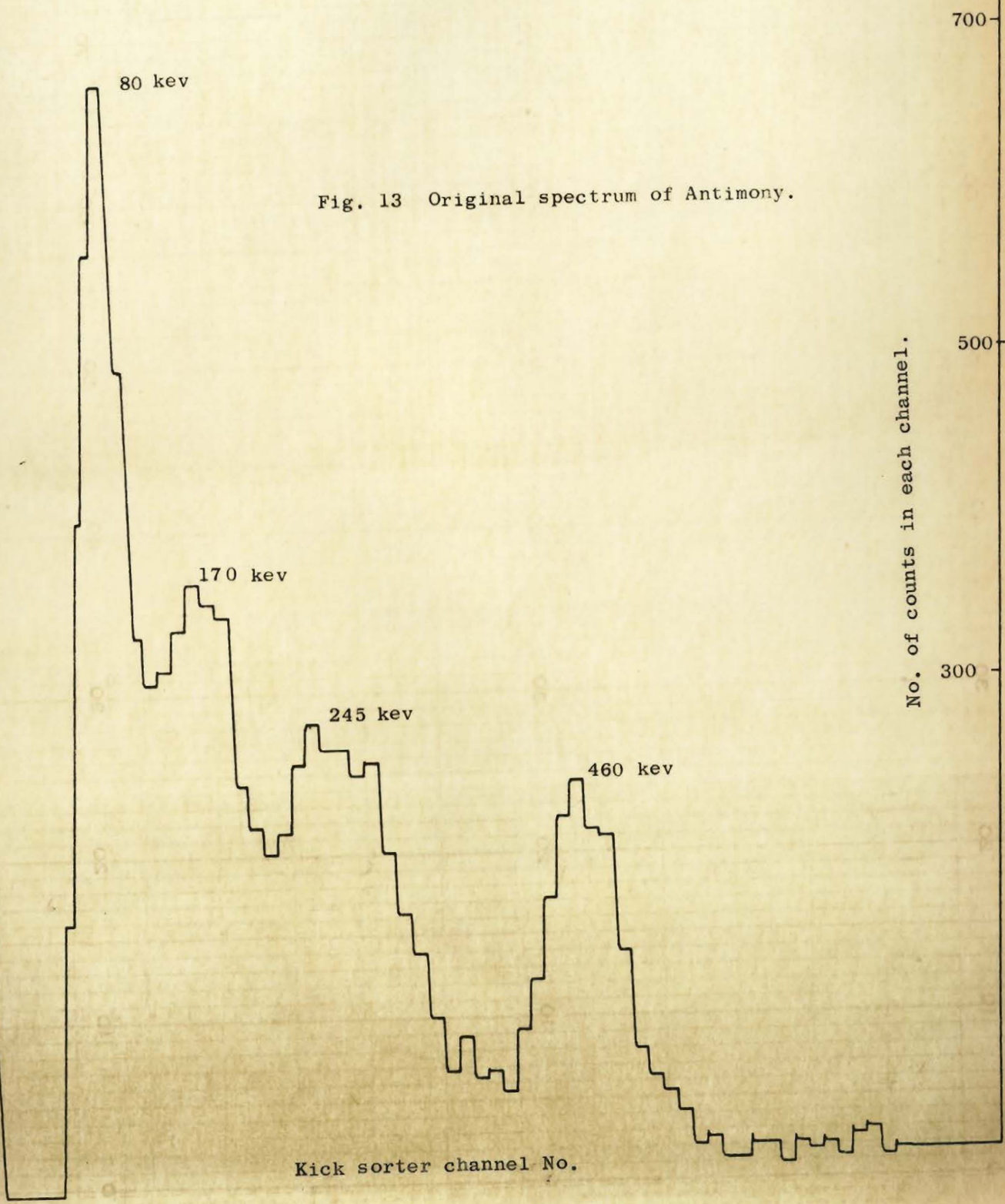


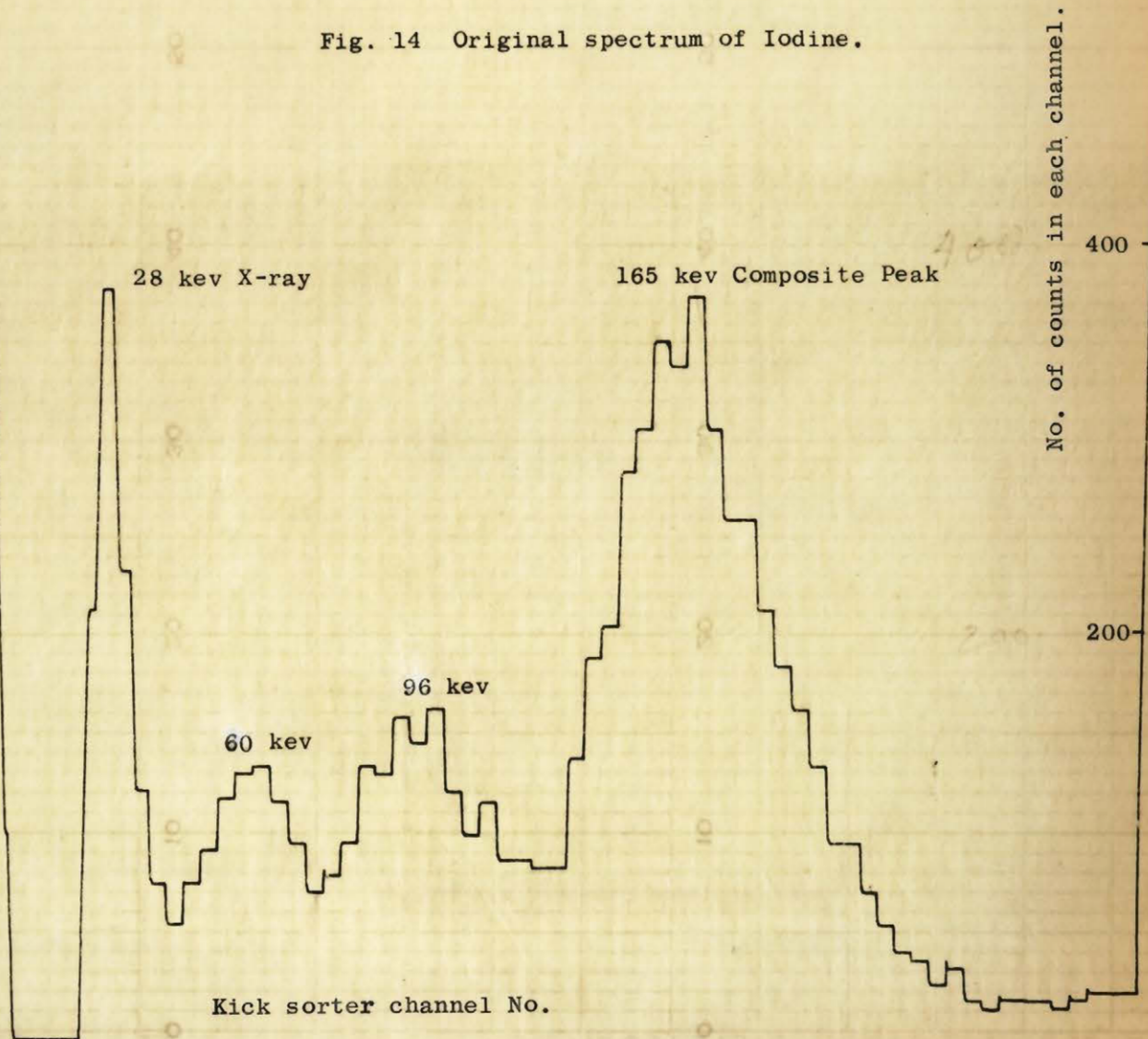
Fig. 13 Original spectrum of Antimony.

Kick sorter channel No.

40,000 pulses

34.

Fig. 14 Original spectrum of Iodine.



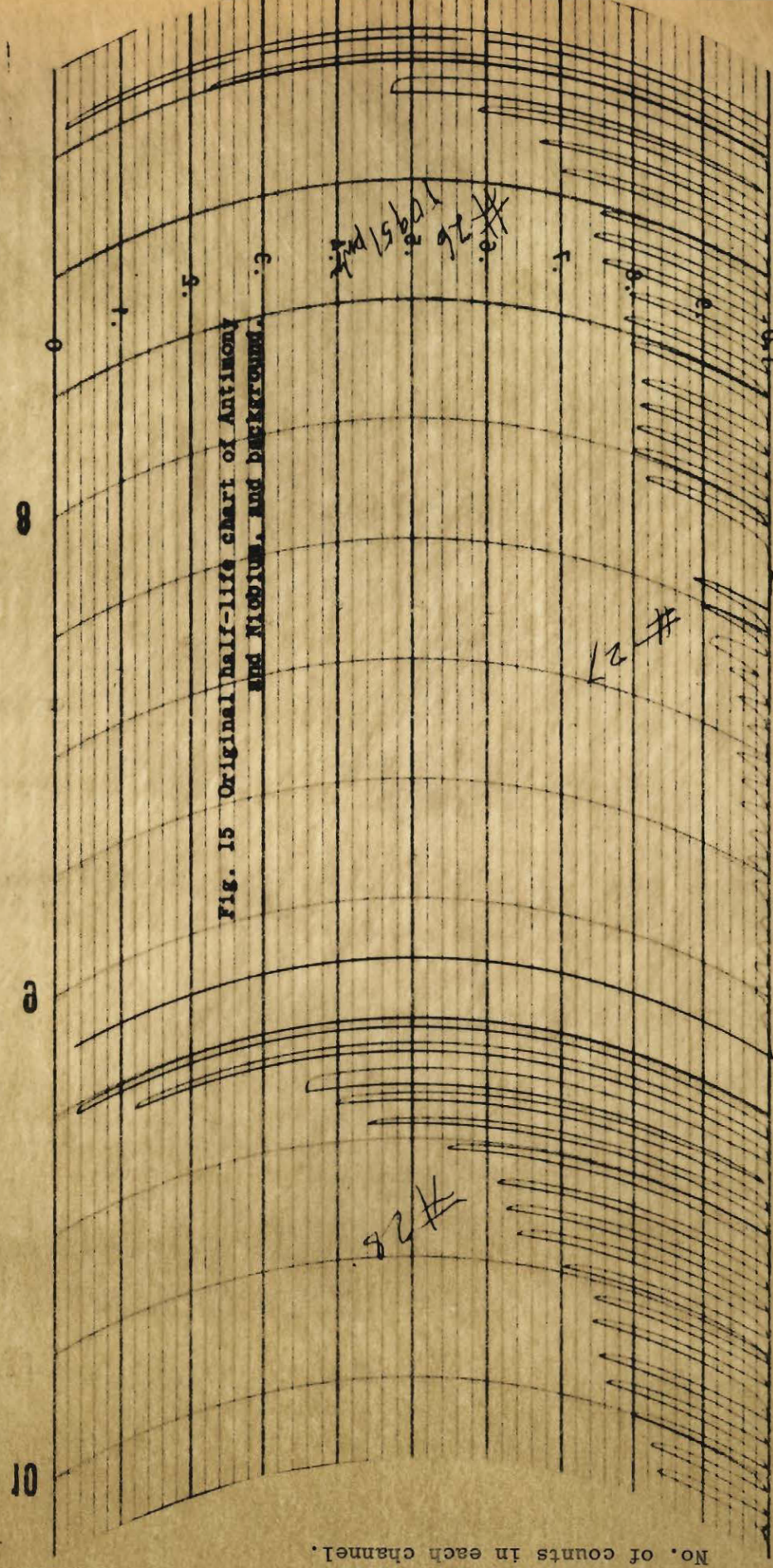


Fig. 15 Original half-life chart of Antimony and Methyls, and background.

No. of counts in each channel.

THE ESTERLINE-ANGUS CO. INC. INDIVIDUALS' IND. P.S.V. CHART NO. 4302-C Integrator channel No.

2. Measurements.

For each target four different measurements were carried out and recorded separately. These were

- a) Half-life measurements.
- b) Energy spectrum.
- c) Shape of energy spectrum as a function of first delay (see Fig. 3).
- d) Yield curve and threshold value for the reaction.

In addition, the critical absorption measurements of the X-rays from Sb and I targets were carried out.

(a) In calculating the half-life, the background associated with the beam itself was recorded for each run and subtracted. The background due to the scattering in the target itself was estimated on each graph and subtracted as shown in each half-life curve. For each case at least six independent half-life measurements were carried out for agreement.

(b) From the energy spectrum the intensity and the energy of the γ -ray corresponding to each peak were determined respectively from the total number of counts under the peak and the position of its line of symmetry in relation to a line of known energy. Under each peak, however, there is the superimposed background which has to be subtracted. The background under a peak is due to the scattered photons associated with the proton burst, the Compton and back-scattered photons from a higher energy peak and photons from any longer-lived activity that may have been induced. The background due to longer lived activity could be faithfully subtracted automatically in the kick sorter, if its half-life is of the same order as the duration of a run (i.e. of the order of one minute). The background due to the beam itself is practically eliminated by allowing

the transients associated with the beam to die out before the phototube starts counting. This is accomplished by the first delay (see Fig. 3). The position and shape of Compton edge and back scattering peak from a higher energy peak to a lower energy one was determined on the graph of the energy spectrum and subtracted from the total number of counts under the peak concerned. If the proper background is subtracted the shape of the peak will resemble a true Gaussian distribution. For better precision in measuring intensity and mean energy, the shape of each peak was plotted on an arithmetic probability graph which is a straight line for a Gaussian distribution. The intersection of this line with the 50% mark defines the mean energy and the slope of the line is a measure of the resolution which can be expressed as:

$$\text{full width at half-maximum} = \frac{1.745 \times 2r}{\text{mid. channel}}$$

where $2r$ is the channel interval between 25% to 75%. Deviations both from the expected resolution (Fig. 8) and straight line relation are indications of non-Gaussian distribution. These two criteria were used as a check against improper background subtraction.

The effect of background activities of the order of seconds was minimized by using a very low pulse repetition frequency of the beam and reducing the counting period to the order of the half-life being studied. The magnitude of the background arising out of seconds order of background activity could be estimated by increasing the first delay to the order of about three half-lives of the isomeric state and increasing the counting period as much as possible. This would by-pass the isomeric state and record mainly the longer activity.

(c) If from the time analysis it was found that more than one γ -ray is associated with the same half-life, an additional check was obtained by

recording the energy spectra for different values of the first delay period. The usual values used were one half-life, two half-lives and three half-lives. If the ratio of intensities of the various peaks stayed constant, then these peaks were associated with γ -rays of the same half life.

(d) The yield curves were obtained by measuring the number of counts under the highest energy peak for the same number of proton bursts as a function of the proton energy. As has been mentioned before the beam energy was reduced by means of graphite absorbers. The principal difficulty was that on reducing the energy of the beam by means of absorbers the quality of the beam was greatly reduced as well. Not only was there a spread in energy introduced (as shown in Fig. 5) but a spread in angle occurred which reduced the fraction of the beam striking the target by an unknown amount. This fact has the effect of making the yield curve rather flat and of displacing the peak toward higher energy. No efforts were made to adjust the yield curves for this effect.

Another method of obtaining yield curves was to measure the number of counts in the first few time channels for the same number of proton bursts as a function of beam energy. By using suitable values of the lower and upper bias levels of the single channel analyser the half-life of any portion of the energy spectrum could be measured. Whenever more than one γ -ray was associated with a single half-life, the half life of each was measured separately by allowing only one γ -ray at a time through the single channel window. This method has the limitation that each channel can accumulate only 1000 pulses, so that points further from the peak of yield have generally low count and comparatively poor statistics. However, the effects of longer-lived background are less serious in this case because

these can be better estimated and subtracted on the graphs as shown (Figs. 22, 23). The yield curves obtained by both these methods are in general agreement.

3. Probable Errors.

The half-life for each isomer was measured on different days, using different channel intervals and first delay time. The estimated probable error, from more than six independent measurements, is 5%.

The probable error for energy evaluations of 80 and 460 keV γ -rays from Sb, 120 keV γ -ray from Nb, and 260 keV γ -ray from Y, as well as the resolved γ -rays (of 160 and 190 keV energy) of I, is within 2%. For the 155 keV yttrium γ -ray, 170 and 240 keV antimony γ -rays and 60 and 96 keV iodine γ -rays it is within 3-4%.

The accuracy of intensity determination depends upon the accuracy of background estimation. The spread in the values of relative intensities from different measurements were taken as a measure of the probable error for intensity measurements and this amounted to about 10%. For 120 keV Nb γ -ray and 460 keV Sb γ -ray the probable error was within 5%.

V. Results.

1. Yttrium. $Z = 39, A = 89, N = 50.$

Proton bombardment of monoisotopic yttrium target resulted in an isomeric state of $27 \mu\text{s}$ half-life, (Fig. 17). Two γ -rays of energies 155 keV and 260 keV were found (Fig. 11). That both the γ -rays were associated with the same half-life was found by measuring them separately by means of the single channel analyser. The peaks associated with the two γ -rays were analyzed for their shape on the arithmetic probability graphs (Fig. 19a, 19b). The resolution of the 260 keV peak has the expected value as can be seen from the resolution-energy relationship in Fig. 8. The resolution of the 155 keV peak, however, was poor. The poor resolution was due to the presence of back scattered and Compton scattered photons from 260 keV γ -ray. The positions of the Compton edge and the back scattering peak for 260 keV γ both happened to be nearly at the position of the 155 keV line. There was evidence also of the presence of an activity of half-life of the order of one second. Both these effects were responsible for poor resolution. The effect from 511 keV long lived activity was subtracted automatically.

No X-rays could be detected due to self absorption in the target and absorption in the 0.005" thick aluminium container of the NaI crystal. The mass attenuation coefficient of aluminium for 14.9 keV yttrium K_{α} X-ray is about $6.5 \text{ cm}^2/\text{gm}$. This alone would reduce the X-ray intensity by 20%. The mass attenuation coefficient of molybdenum for 15 keV X-ray is $22.0 \text{ cm}^2/\text{gm}$. For yttrium this value would be somewhat higher. Therefore an effective target thickness of even .005" would absorb nearly 80% of the X-rays produced. Thus the atomic number of the isomer could not be determined by critical absorption of X-rays and the reaction type was unknown, since, in addition,

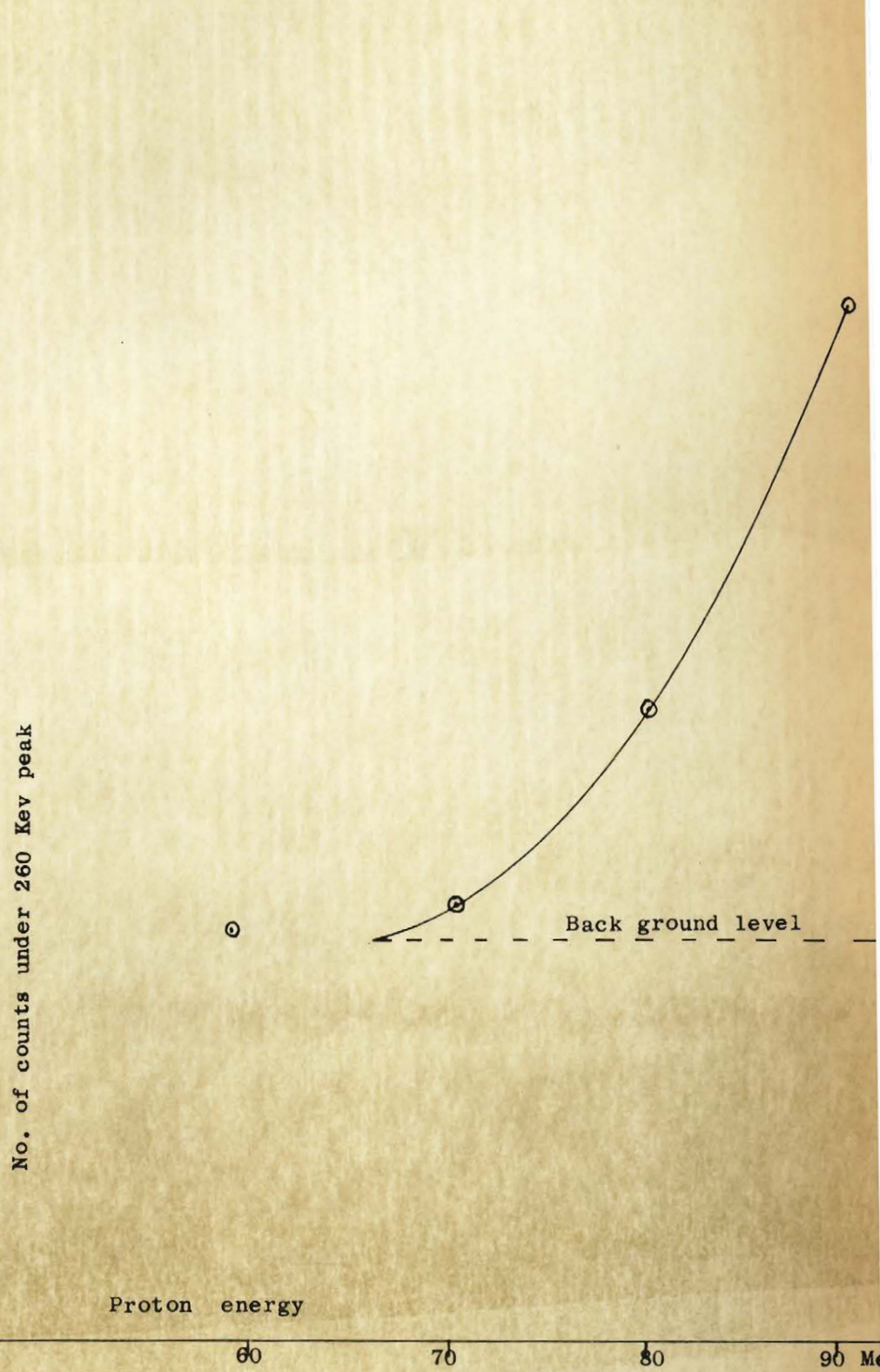


Fig. 16. Yield curve of yttrium target.

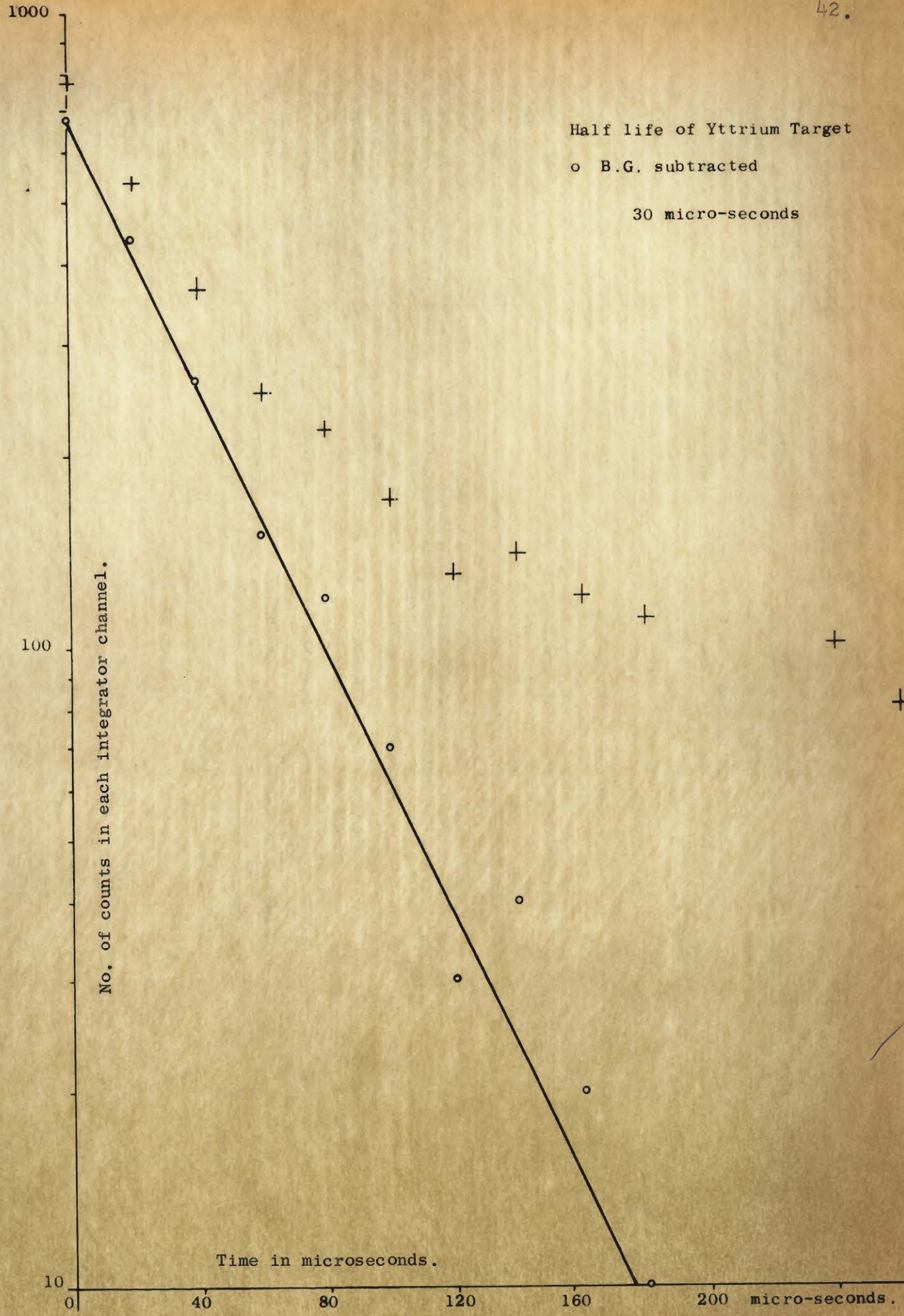


Fig. 17

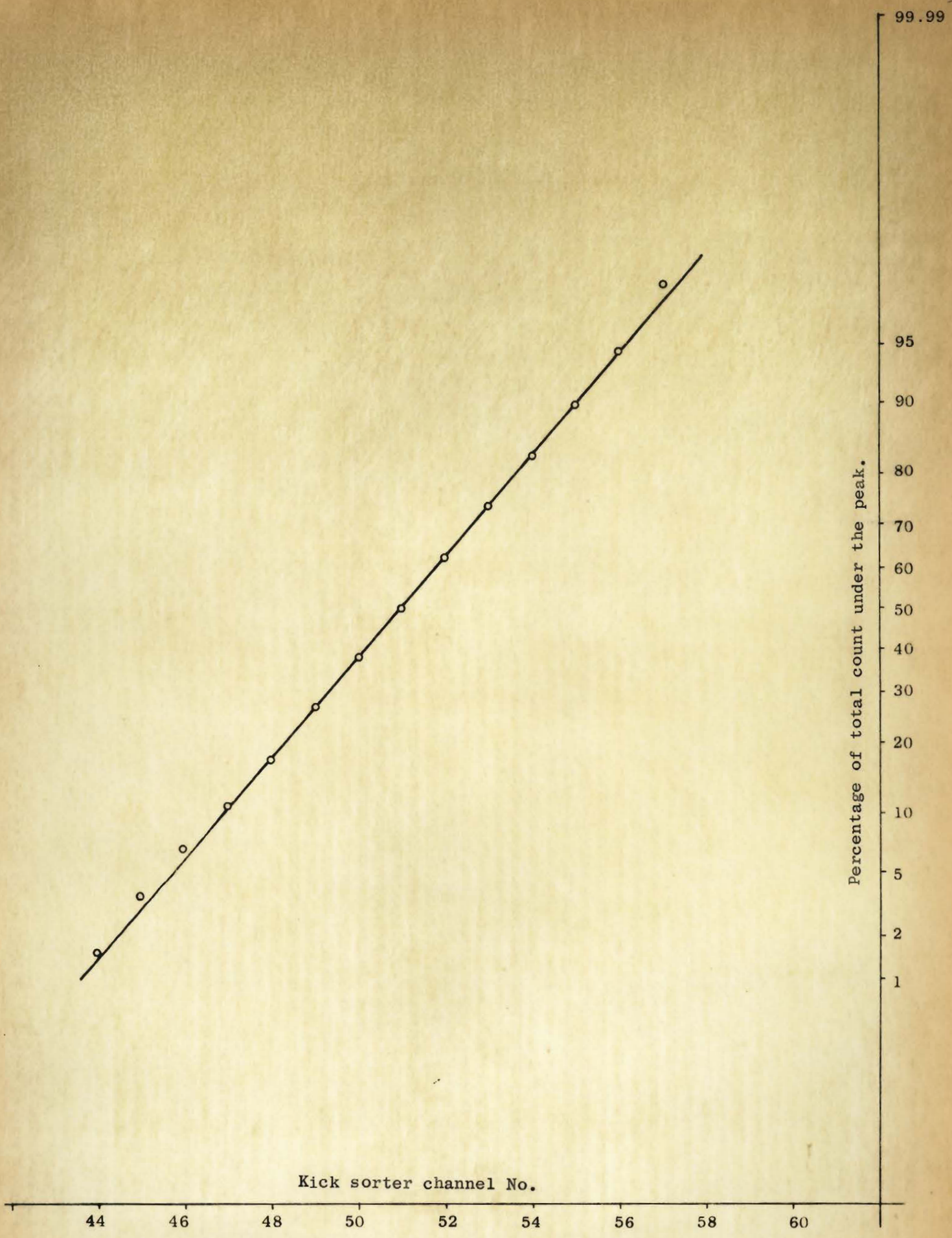


Fig. 18 Gaussian distribution of 511 kev line of Na²².

155 kev
Resolution 40%

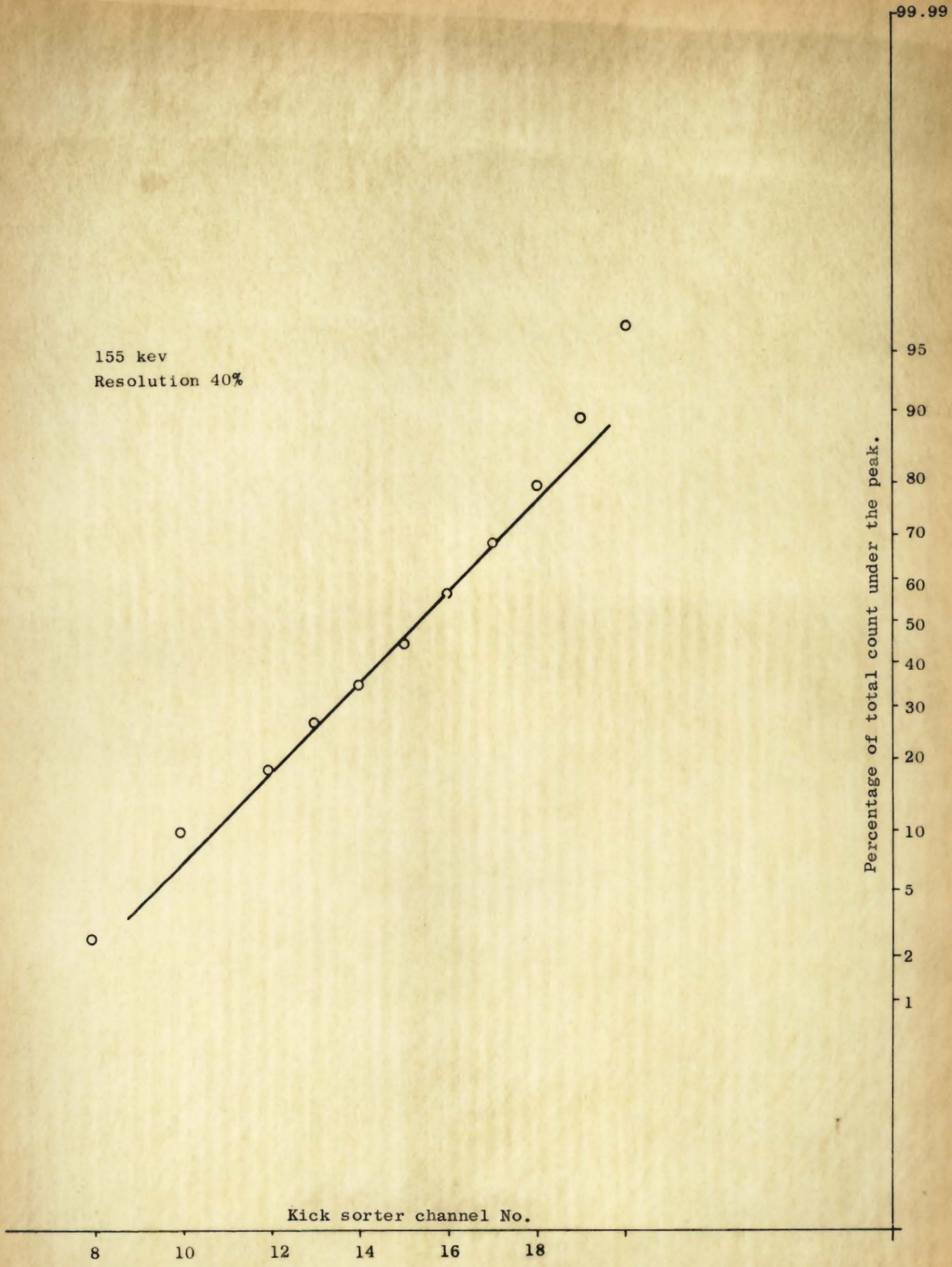


Fig. 19A Gaussian distribution of 155 kev line of Yttrium target.

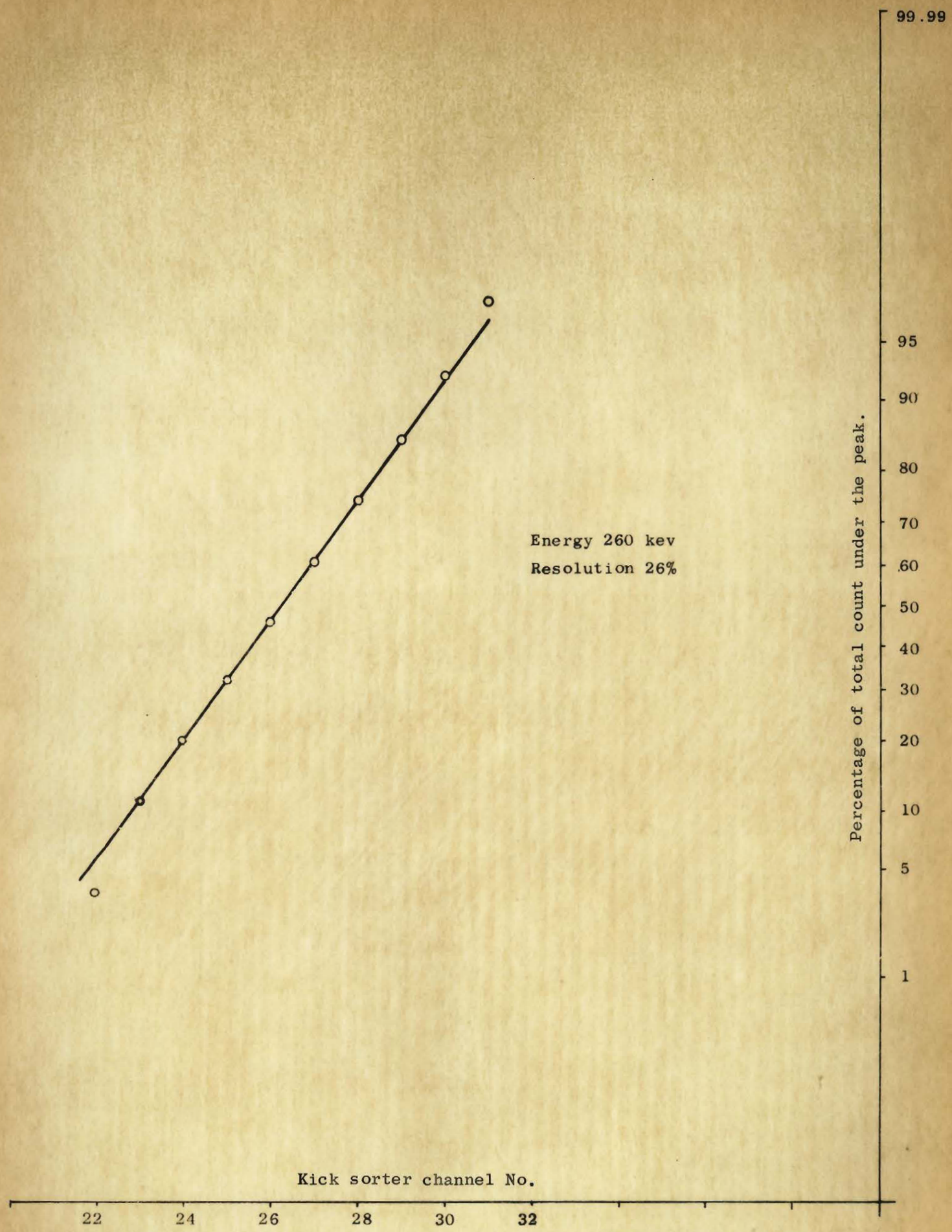


Fig. 20 Gaussian distribution of 260 kev line of Yttrium target.

it was not possible to bombard the neighboring elements Sr and Zr.

Further, the yield curve/obtained ^{Fig. 16 p. 41} was also unsatisfactory mainly because of secondary activity already referred to for which adequate correction could not be made. However the threshold for production of the 27 microsecond activity appears to be in the neighbourhood of 60-70 Mev.

From the number of counts under the two peaks corresponding to the 155 kev and 260 kev γ -rays and their respective counting efficiencies (Fig. 9) the relative observed intensities were computed.

The probable multipolarities of both the transitions would be M2 for 27 μ s half-life according to Weisskopf's estimates. In the absence of any information about X-ray intensity, there was no way to check the internal conversion coefficients. However an attempt could be made to suggest a decay scheme solely on the basis of the observed intensities of the two γ -rays.

The two possibilities of cascading (Fig. 41(a)) are: Either 150 kev is an M2 transition with a half-life of 27 μ s followed by a prompt 260 kev transition of lower multipolarity. From Table II a the ratio of intensity of 260 and 150 kev γ -rays is 1.38, and the total internal conversion for 150 kev M2 transition is 0.43. Then by matching the populations of the two states one gets the relation:
$$\frac{N_1}{N_2} = \frac{1 + \alpha_2}{1 + \alpha_1}$$

conversion for the 260 kev γ -ray, which satisfies this relation, is

$$1 + \alpha = \frac{1.43}{1.38} = 1.036. \text{ From table of internal conversion coefficients (13)}$$

$\alpha_2 = 0.033$. Thus a 260 kev E2 would fit this scheme.

Or the 260 kev is an M2 transition followed by the 150 kev γ -ray. The total internal conversion coefficient for 260 kev M2 is 0.067 and the total population of this state would be $(1 + 0.067) \times 1.49 \times 10^5 = 1.59 \times 10^5$.

The population of the 150 keV state should be equal to this as well.

This requires a total internal conversion coefficient of 0.54. From the table (13) the total value of β_2 for 150 keV is 0.43.

Thus both these alternates seem possible but an M2 - E2 cascade will be preferred over an M2 - M2 one because in the second case the half-lives will hardly differ, and further there would be two changes of parity.

It may be worth observing that the ground states of odd-even yttrium isotopes of mass 93, 89, 87 are assigned as ($1/2^-$). Now if we adopt the preferred M2 - E2 scheme, the levels in the new isomer will be respectively ($1/2^-$), ($5/2^-$) and ($9/2^+$). These assignments are consistent with the shell model for even-mass isotopes of yttrium.

2. Niobium. $Z = 41$, $A = 93$, $N = 52$.

Proton bombardment of .025" niobium target yielded a single γ -ray of 120 keV energy (Fig. 12) and a half-life of $65 \mu\text{s}$ (Fig. 23). The peak corresponding to this γ -ray was analyzed for its shape and the resolution when compared with the graph in Fig. 8 indicated a simple peak.

No X-ray was found even with a target of .005". The same arguments, and nearly the same values as for yttrium, could be used to show that an estimated 90% attenuation of 16 keV X-rays would result from absorption in the target itself and in the aluminium container of NaI crystal.

The yield curve for the reaction was obtained by both the methods outlined in the procedure of measurements (Figs. 21 and 22). These two yield curves agree quite well with each other. The type of reaction could only be estimated from the shape of the yield curve and the threshold of the reaction as the Z value of the isomer could not be determined. A (p, 4n) reaction would give a mass difference equal to the threshold value of 30 MeV; and on the basis of this alone the suggested reaction would be:

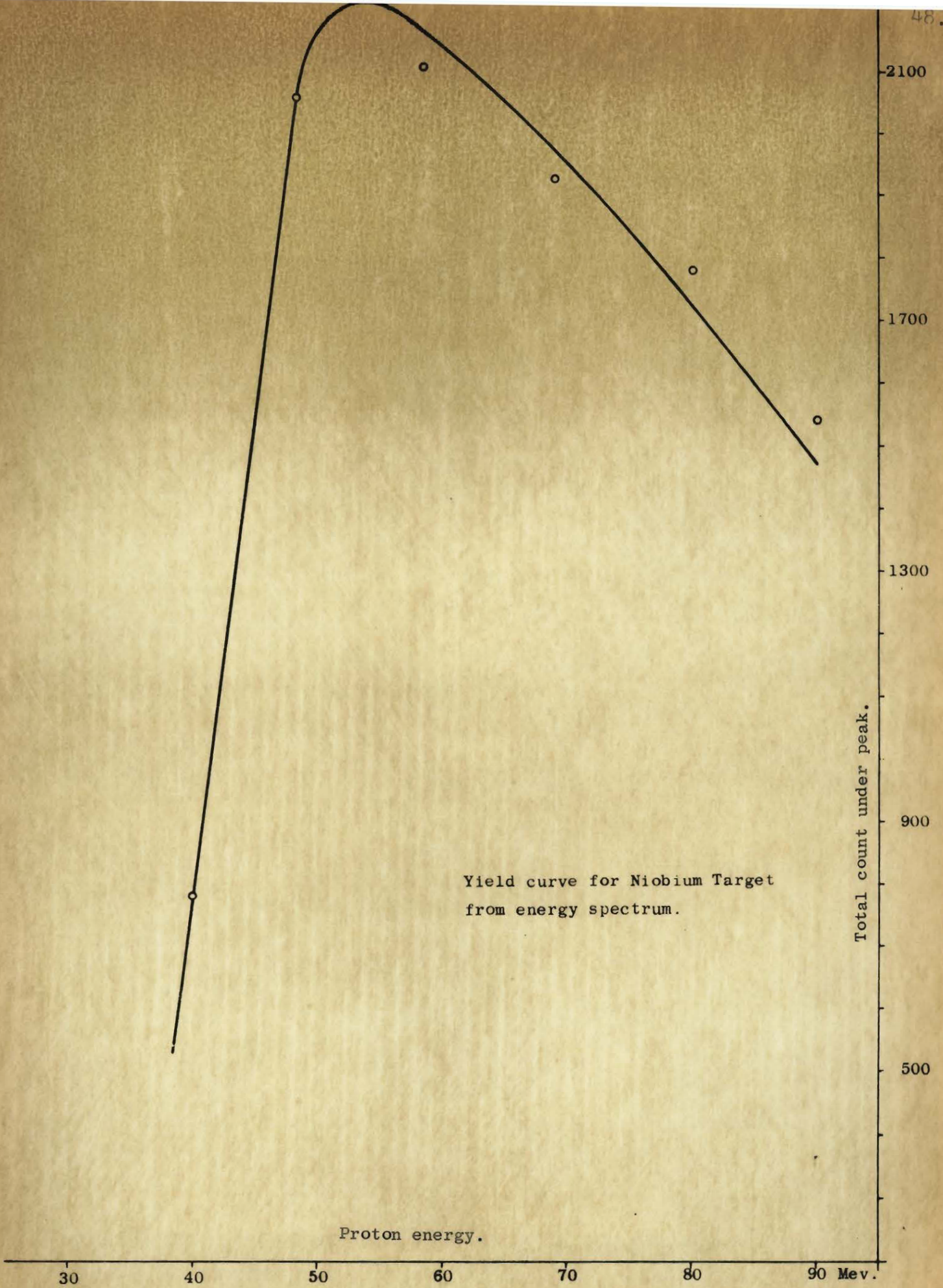


Fig. 21

Yield curve of Niobium target from the first three channels of the 17 channel integrator.

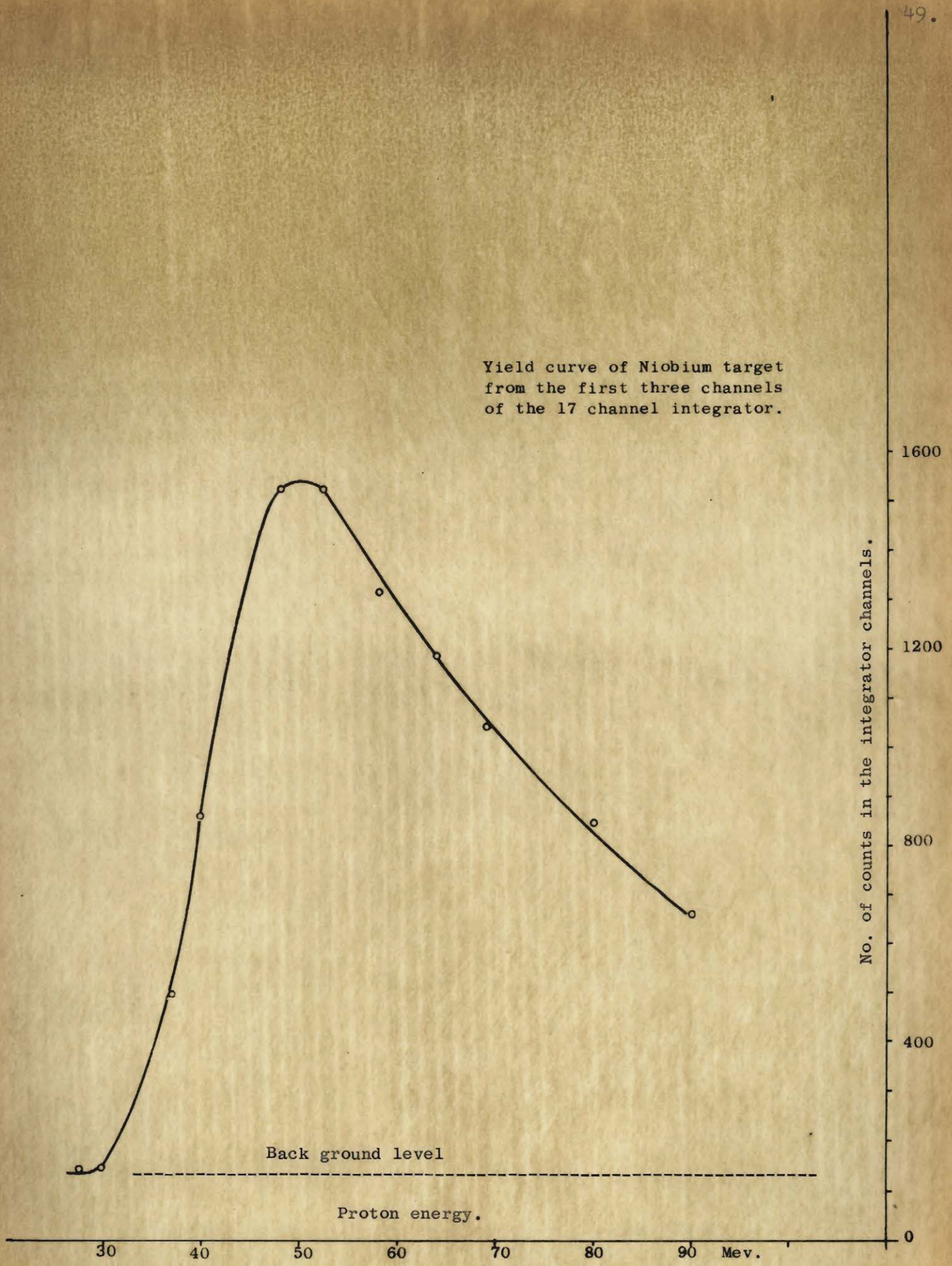


Fig. 22

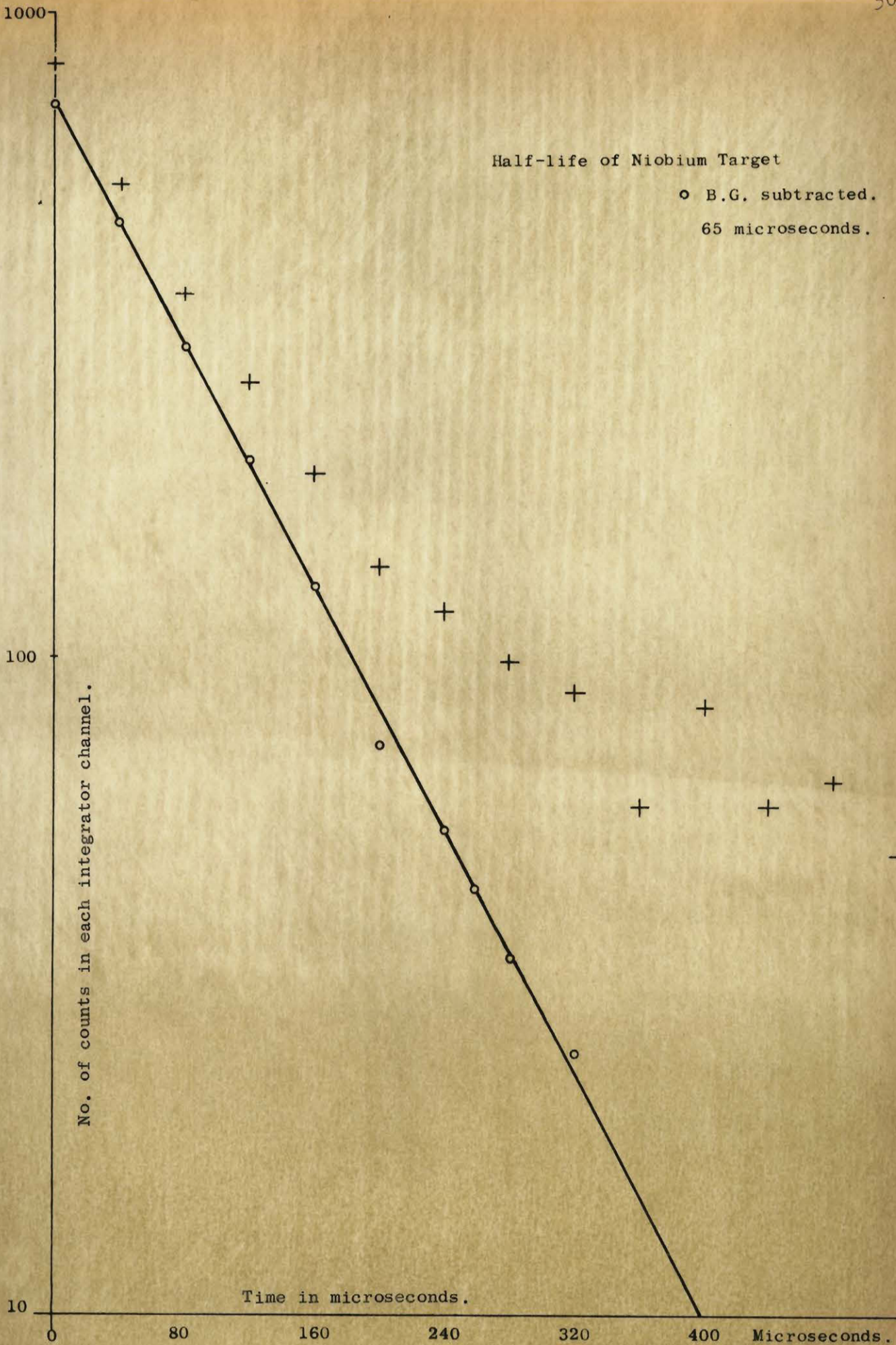


Fig. 23

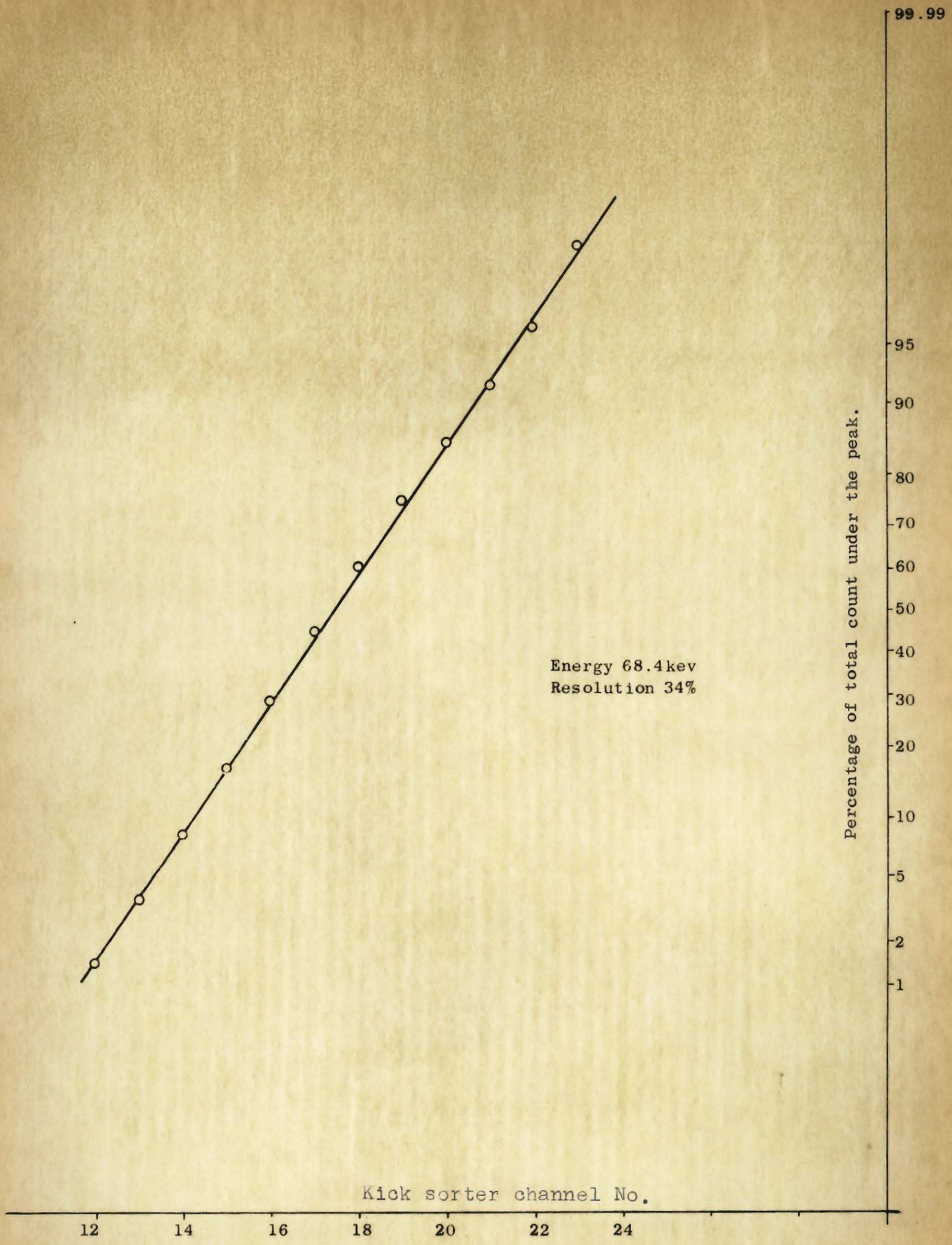


Fig. 24 Gaussian distribution of 68.4 keV calibration line.

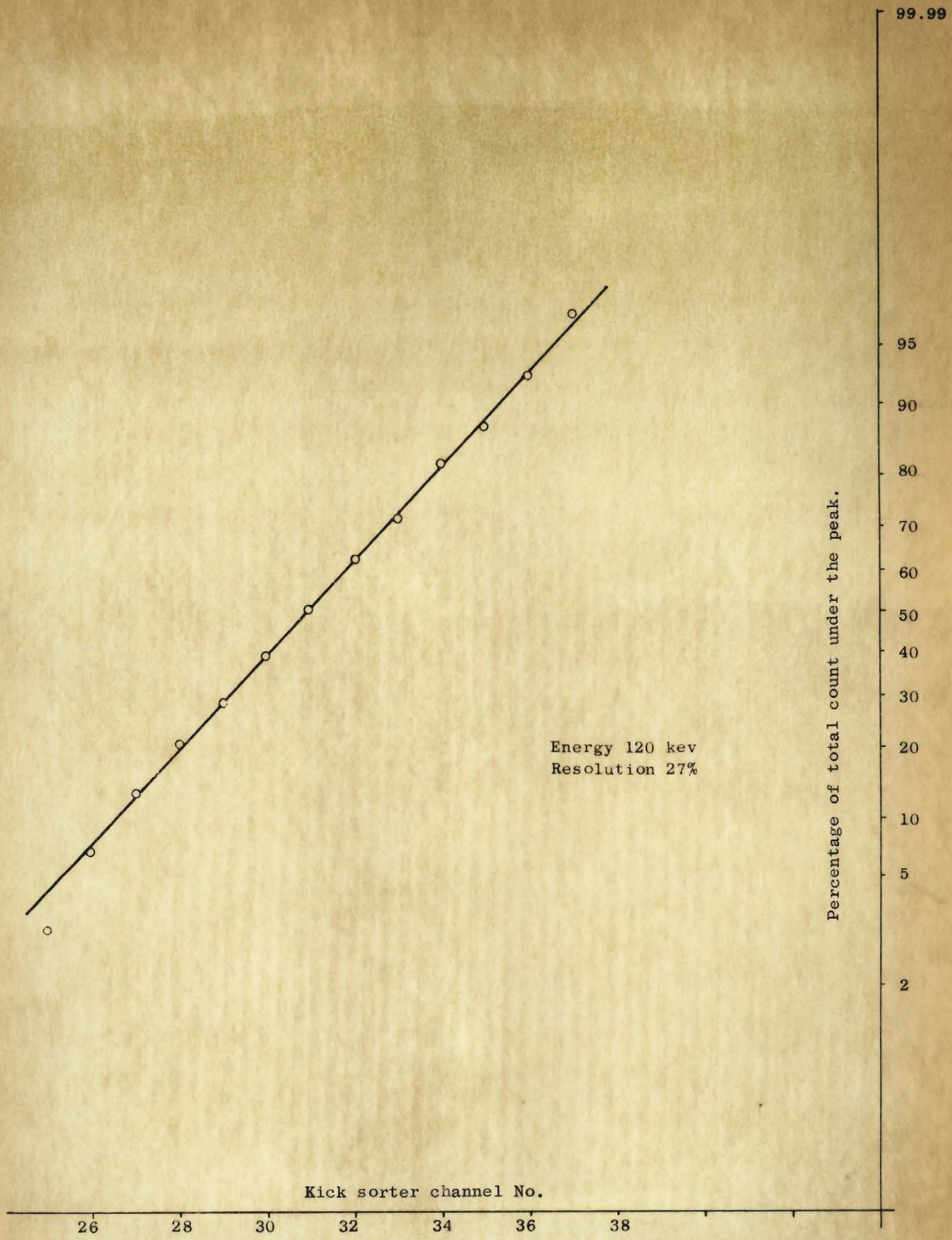


Fig. 25 Gaussian distribution of 120 kev line of Niobium target.

The method was to subtract the 511 keV spectrum (of Na^{22}) from the spectrum of the isomer. First a spectrum from antimony target was stored in the kick sorter. The gain was then changed to make the 511 keV γ -ray occupy the same channels as the 460 keV one. The subtraction was continued until the 460 line disappeared. This procedure would subtract satisfactorily the back-scattering peak and the Compton background of 460 keV γ -ray from the antimony spectrum. But the peaks at 170 and 245 keV still persisted, although reduced, thus establishing the existence of primary γ -rays corresponding to these energies.

That these two γ -rays also had the same half-life as the 80 keV and 460 keV ones was established by the fact that the relative intensities of all the four γ -rays remained substantially unchanged for values of the first delay time from $80 \mu\text{s}$ to $500 \mu\text{s}$. (See Fig. 3).

The shape and resolution of the peaks corresponding to the 80 keV and 460 keV γ -rays were obtained on the arithmetic probability graphs (Fig. 30 and 31 respectively). The shape of the 460 keV peak was found to correspond satisfactorily to a Gaussian distribution and the resolution agreed with the expected value, as shown in Fig. 8. The resolution of the 80 keV peak, however, was poor and ^{of} greater than expected value. Apart from the presence of scattered photons from the three higher energy γ -rays, the target thickness would certainly broaden the peak of the softest of the four. The Gaussian analysis of the 170 keV and 245 keV peaks showed some departure from a straight line at the ends because the background varied steeply from channel to channel under these peaks and could not be estimated for each channel separately. But the total background could be estimated more accurately from the Na^{22} subtraction experiment described above. The lack of straight line plots on probability graphs makes the energy assignments

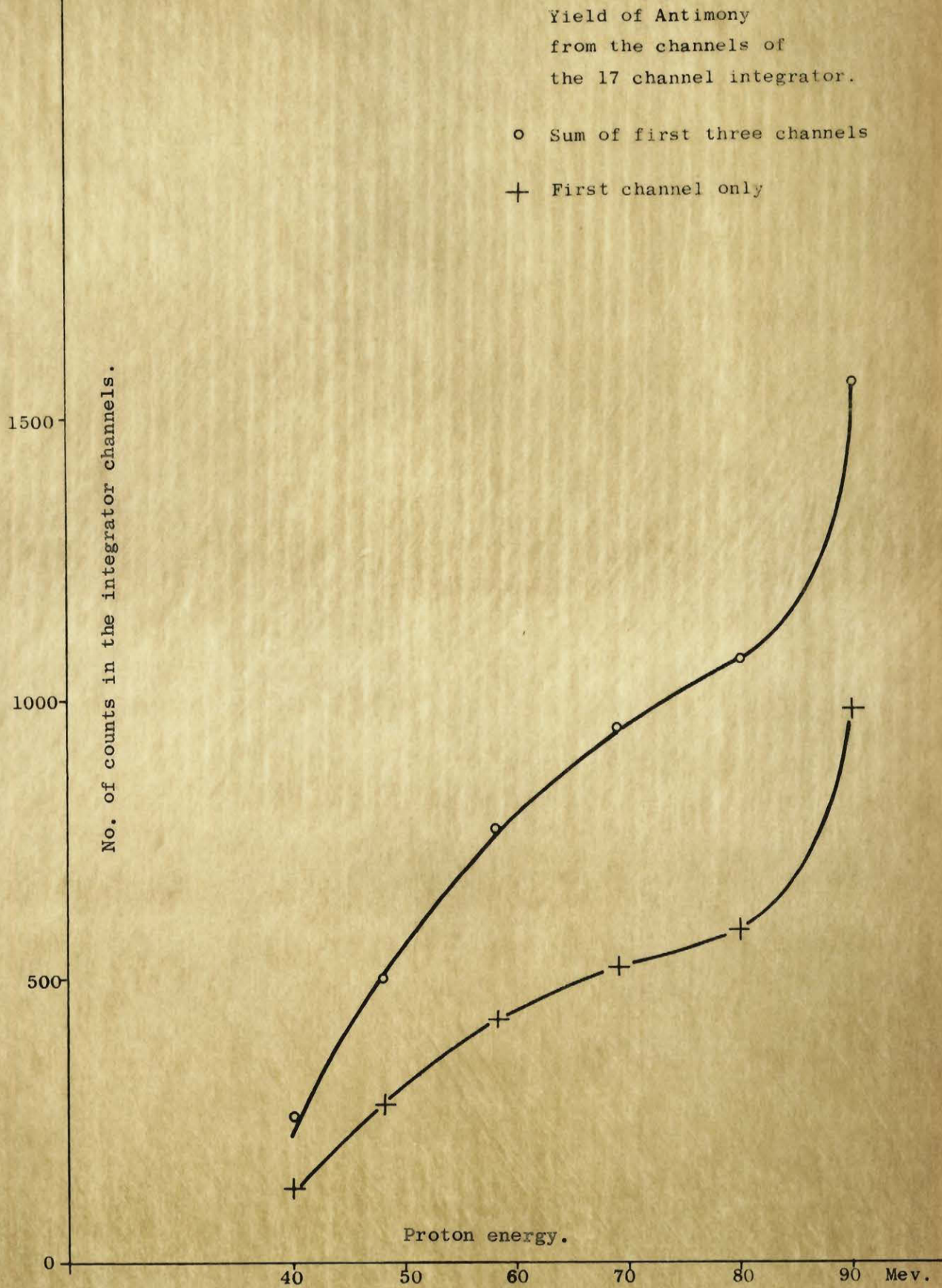


Fig. 26

Yield curve of Antimony
460 kev line only
from energy spectrum.

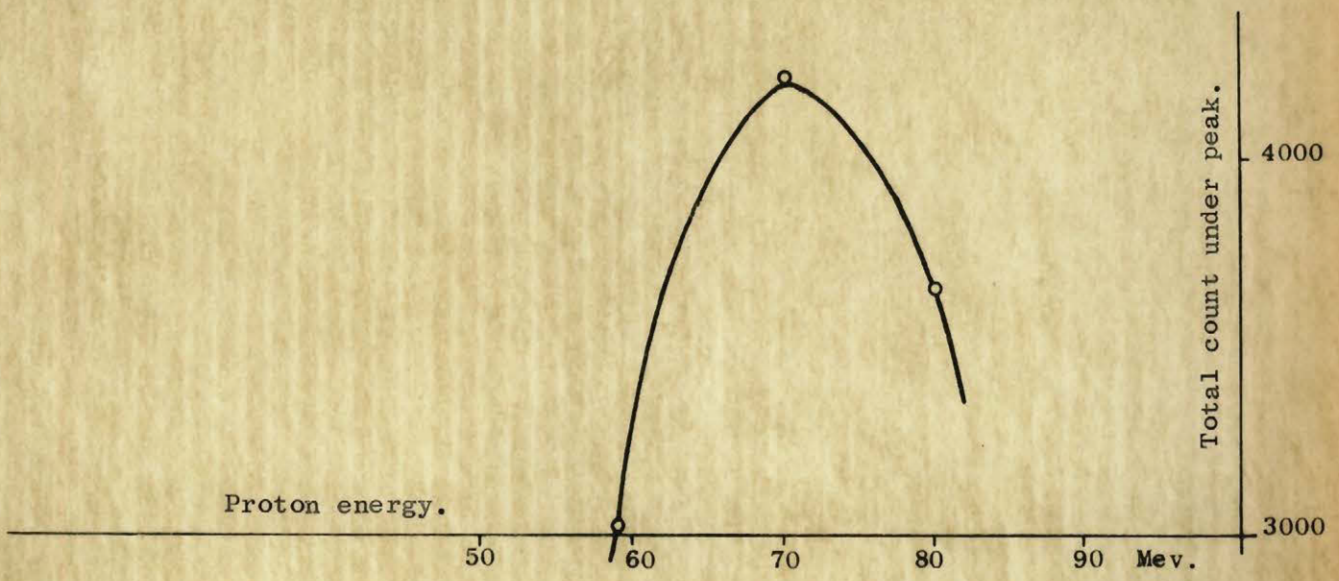
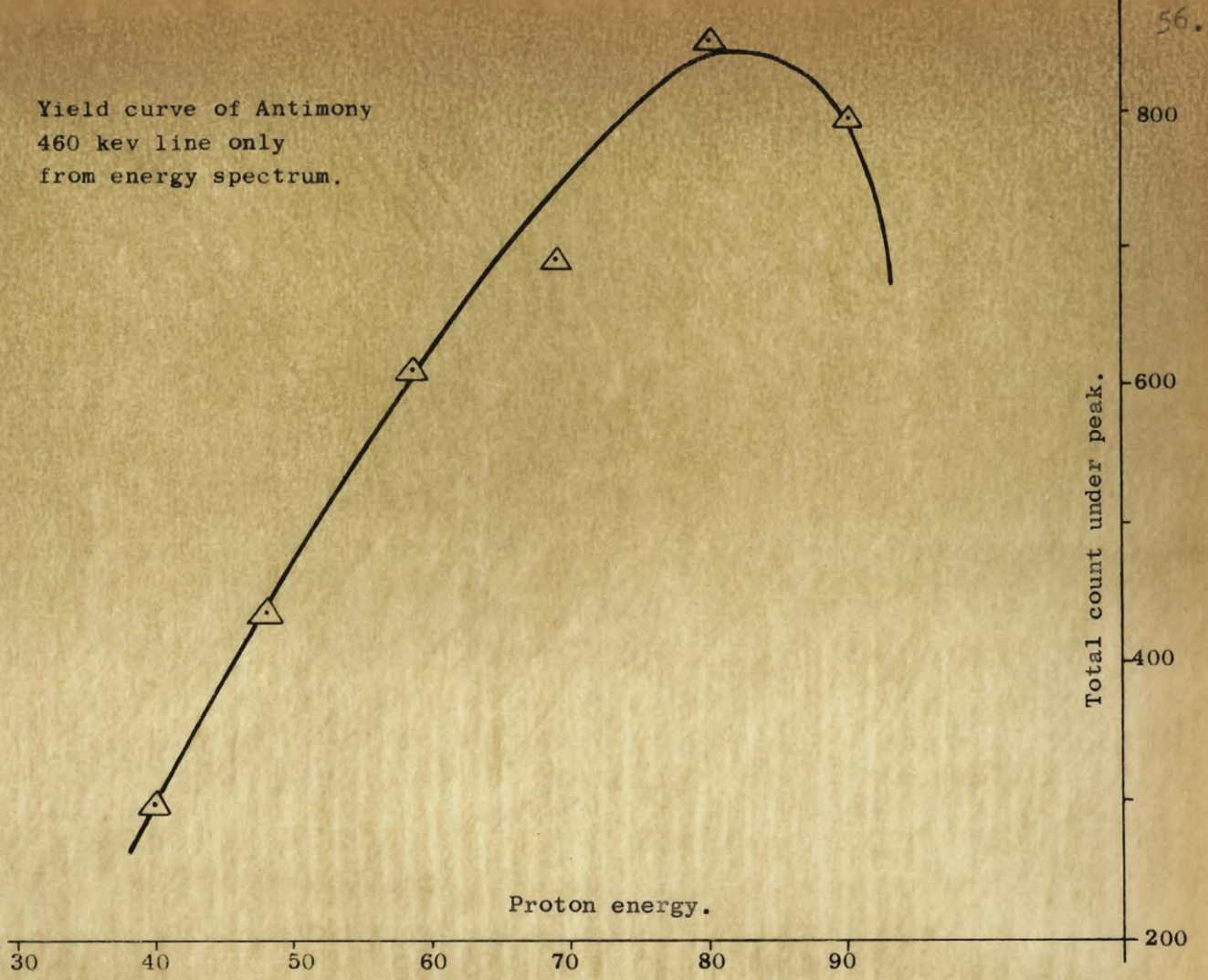


Fig. 27

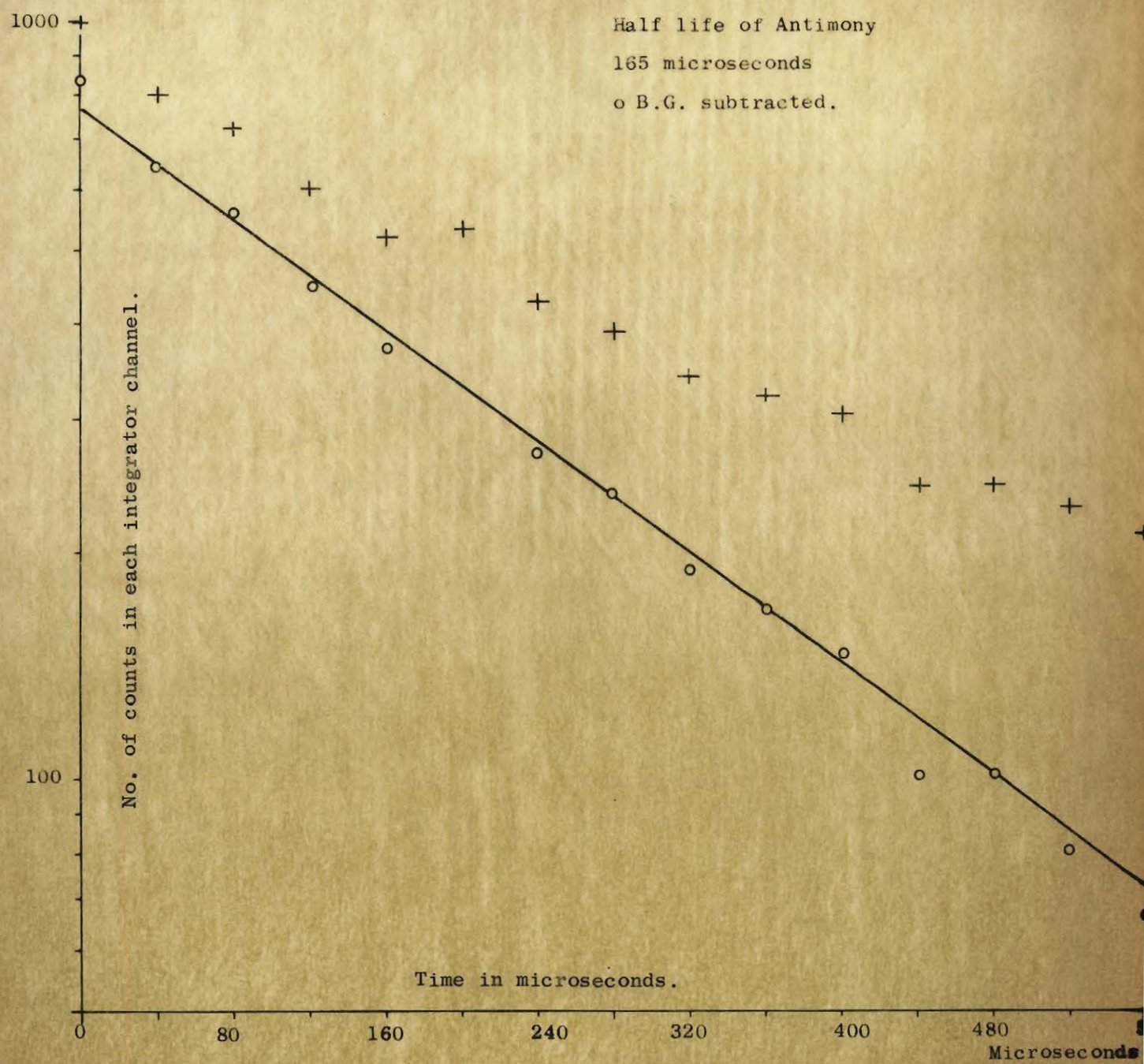


Fig. 28

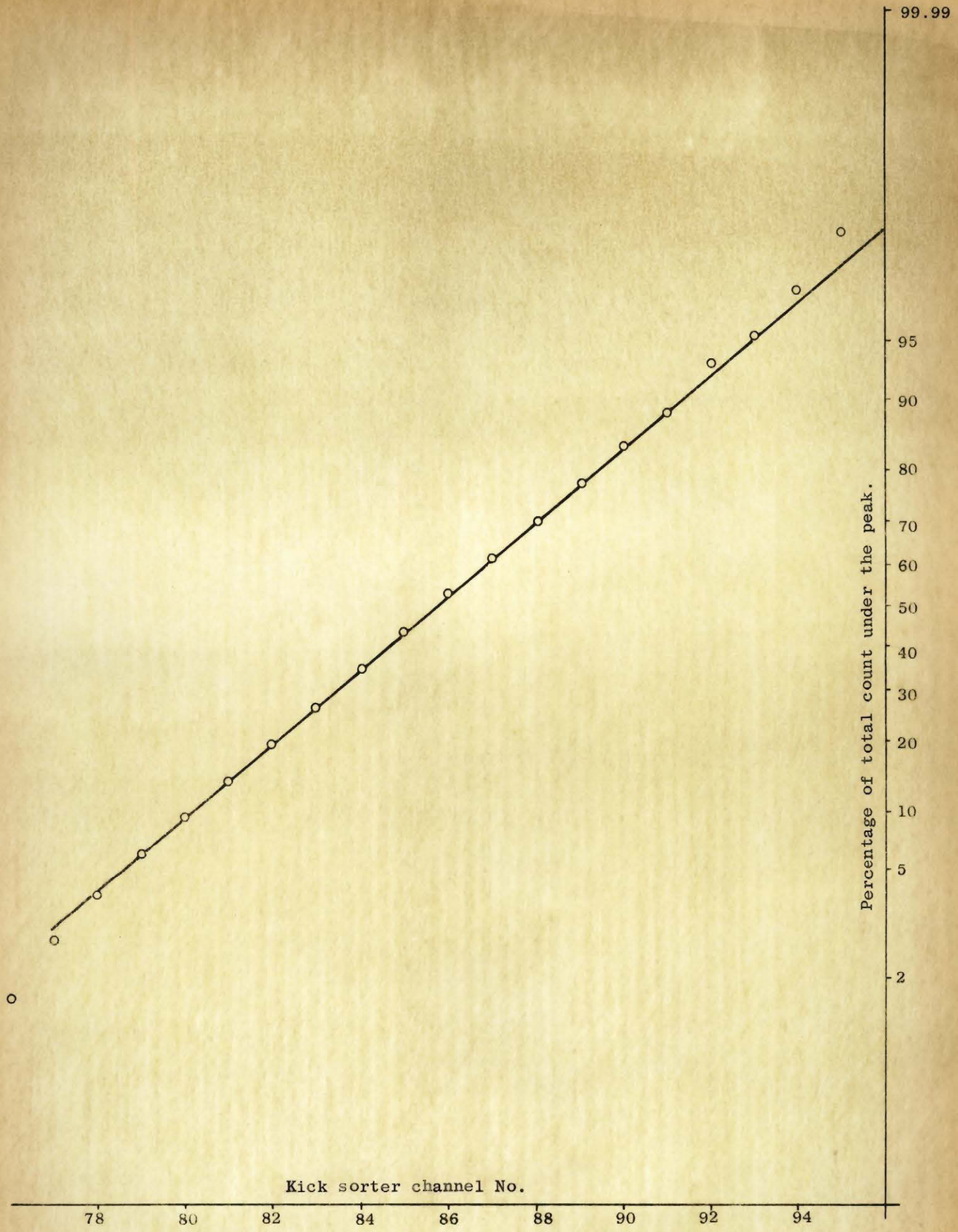


Fig. 29 Gaussian distribution of 662 kev line of Cs137.

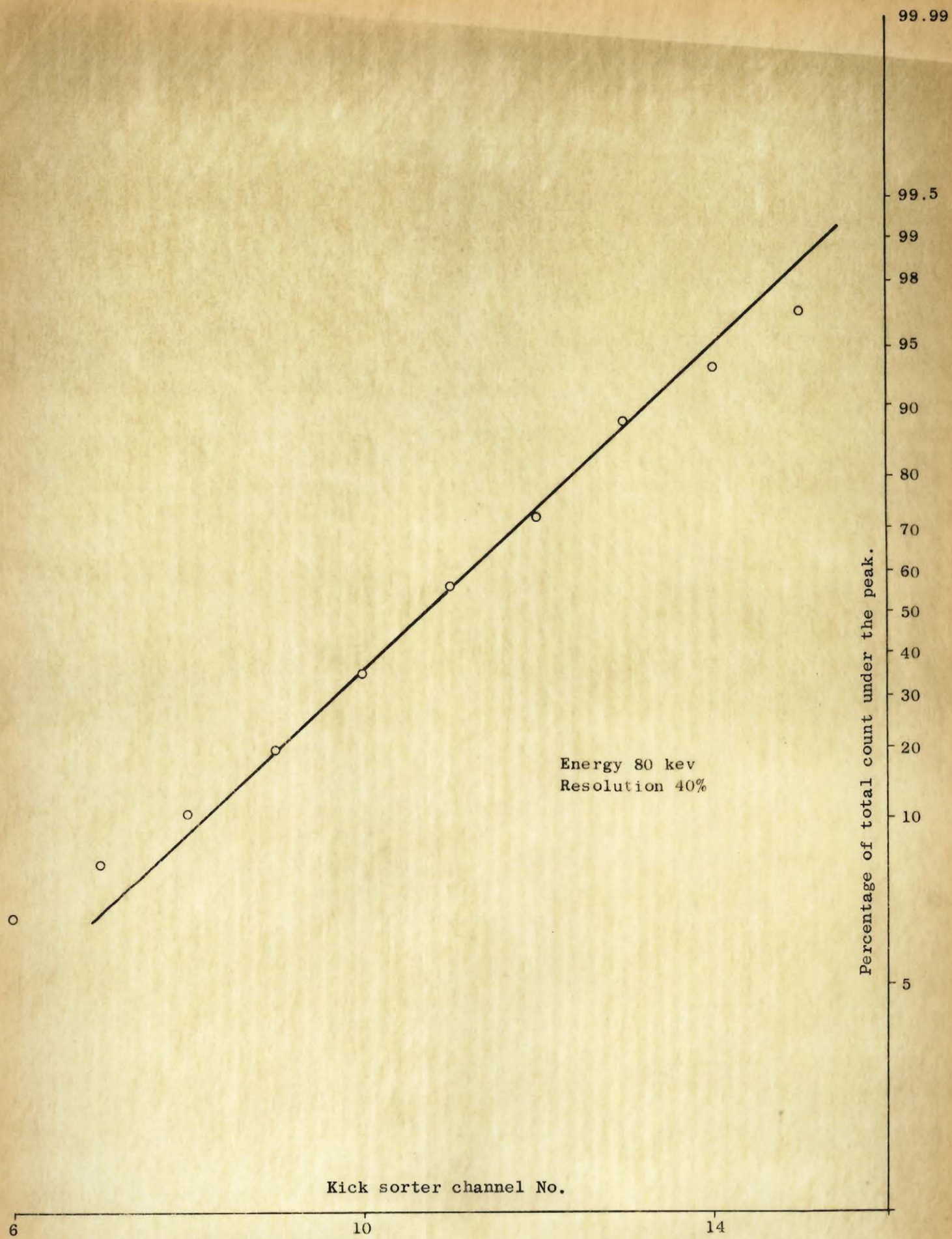


Fig. 30 Gaussian distribution of 80 kev line of Antimony.

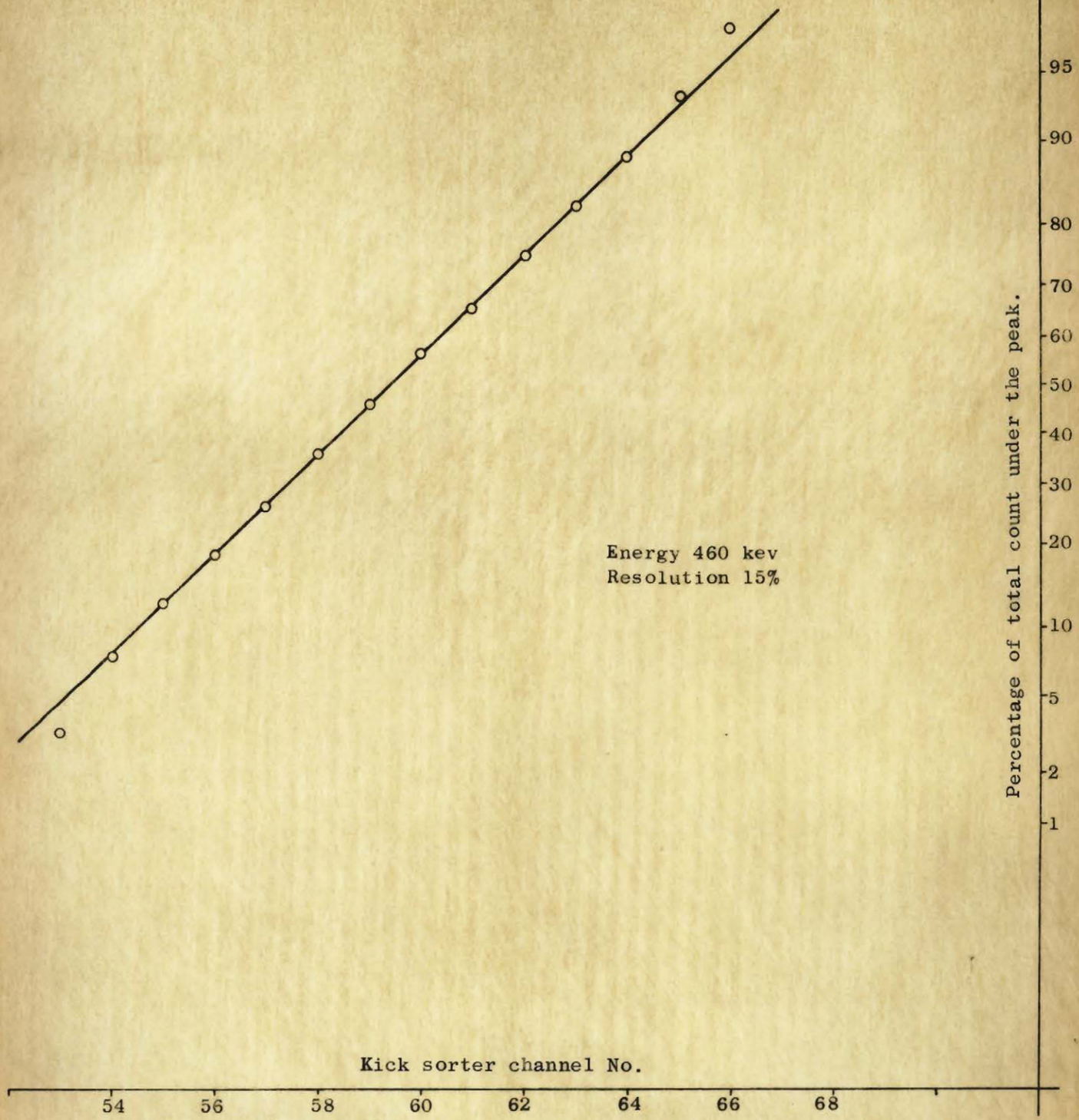


Fig. 31 Gaussian distribution of 460 kev line of Antimony.

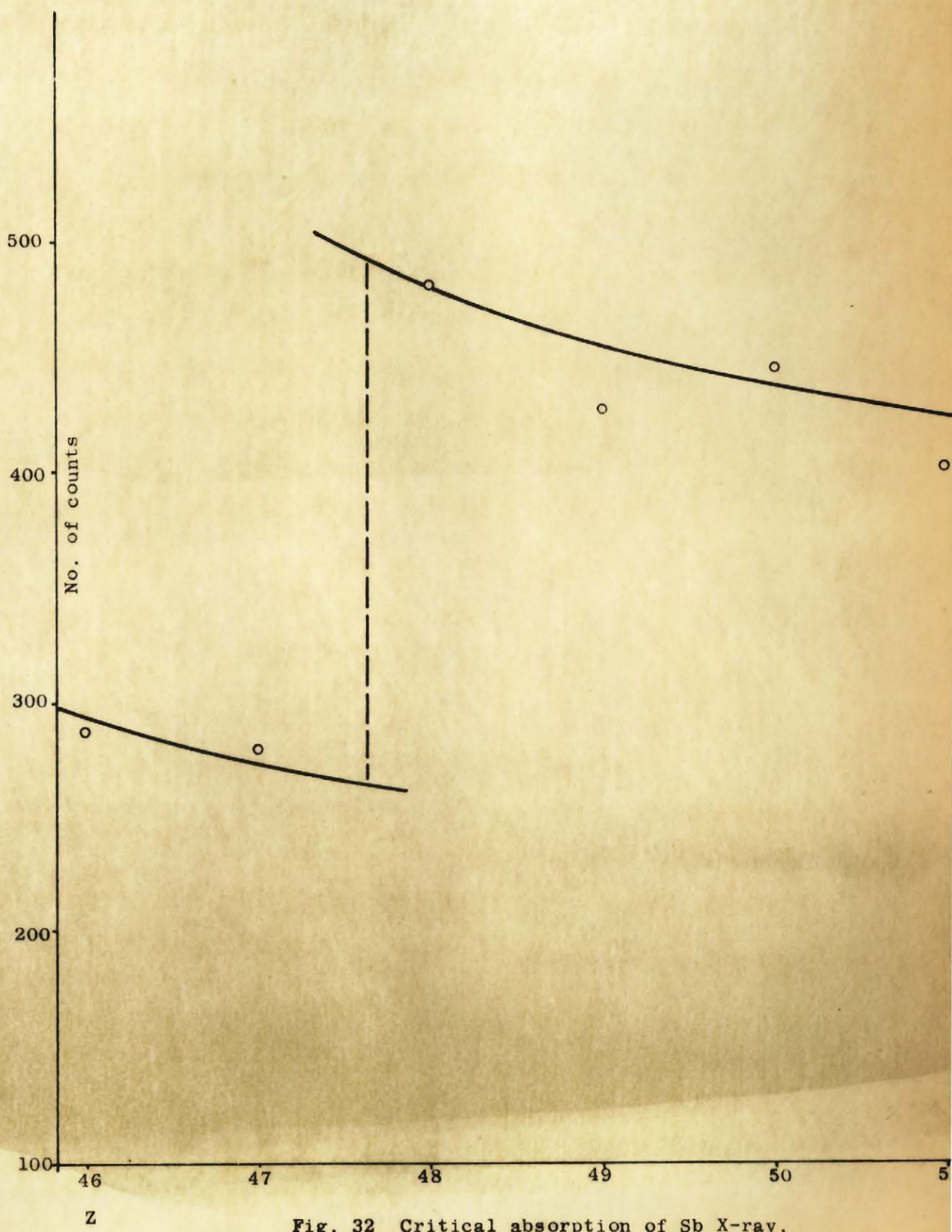


Fig. 32 Critical absorption of Sb X-ray.

of these two γ -rays somewhat less accurate than the other two. The effect of a long-lived activity of half life about 4 minutes was automatically subtracted in the kick sorter from those energy spectra which were intended for intensity measurements of the peaks. Shorter-lived backgrounds can be minimised by using shortest possible counting time. The background corresponding to the 460 keV γ -ray under the peaks of the other three were carefully estimated for relative intensity measurements. The constancy of the ratio of intensities was taken as a measure of the accuracy of background estimation for these four peaks. Source absorption and absorption in the NaI container were taken into account for intensity measurements.

Again the yield curves were unsatisfactory, partly because of difficulties of subtraction and partly because two isotopes are present in about equal amounts. Nevertheless a trace of the 460 keV γ -ray is just visible in the spectrum at a nominal 30 MeV bombarding energy. Using the data from the Table of Atomic Masses of Metropolis and Reitwiesner (10) the threshold for the reaction $\text{Sb}^{121} (p, p4n) \text{Sb}^{117}$ is found to be 32 MeV. Since the spread in beam energy after degradation to 30 MeV is at least 4.3 MeV and since the values from reference (10) differ by about 1 MeV from those given by Halsted (11), it is proposed that the isomer is Sb^{117} .

The X-rays arising out of the K-conversion of the γ -rays was observed (Fig. 32). The critical absorption of the X-rays established the Z-value of the isomer as 51 (Fig. 32) The reaction, therefore, was a (p, p α n) type.

Possible values of the multipolarities of the four lines were estimated from Weisskopf's chart associating each in turn with the observed half-life. For the possible decay schemes, the total K-conversion and the relative population of states in cascade were compared against the experimentally observed values of the intensities of X-rays and the four γ -rays. The

The decay scheme shown in Fig. 41 (b) is suggested on the basis of

- 1) Energy agreement among the lines.
- 2) Agreement between the theoretical values of the K-conversion coefficients, and the measured X-ray intensity.
- 3) The agreement between the expected population of each state with the relative intensities of each line measured and the multipolarity assigned.
- 4) The assignment of multipolarity to each line is in agreement with Weisskopf's estimates within their limits.
- 5) Agreement with single particle level scheme.

Numerous other decay schemes have been investigated but none of these except the suggested one satisfy all the five points discussed above.

The agreements between the measured and assigned values are shown in Table III. The relative intensities of the four γ -rays and the X-ray were measured in two steps. The ratio between the X-ray and the 80 keV peak was obtained from one measurement, Table III (a); and the relative intensities of the four γ -rays were obtained separately, Table III (b). This was to avoid using the entire energy range from 28 keV to 460 keV in one measurement.

The ground state of ${}_{51}^{117}\text{Sb}$ is a $d\ 5/2^+$ state (9). On the assumption of a $(p, p4n)$ and the suggested decay scheme (Fig. 41 (b)) the spins and parities of the levels involved are due to the single odd proton and are as shown in Fig. 41 (b).

It is seen from Table III (b) that the No. of total K-conversion = 1.76×10^5 and the $\frac{\text{number}}{\%}$ of X-rays expected = 1.5×10^5 (reduced by fluorescence yield). Observed $\frac{\text{number}}{\%}$ of X-rays = 1.79×10^5 . Also $n_{80} \simeq n_{170}$ and $n_{170} + n_{245} \simeq n_{460}$.

4. Iodine. $Z = 53$, $A = 127$, $N = 74$.

Iodine target consisted of two $1/16$ " thick polystyrene plates in each of which a $(2 \times 1.5 \times 0.16)$ cm³ groove was machined. Finely divided iodine crystals were firmly packed in the hollow between the two polystyrene sheets and the sheets were cemented together. The thickness of the iodine layer was 0.16 cm.

The isomer, resulting from proton bombardment of the mono-isotopic iodine target, had a half-life of 80 μ s (Fig. 35). The energy spectrum consisted of peaks corresponding to four γ -rays of energies of 60 keV, 96 keV, 160 keV and 190 keV, together with the X-ray peak (Fig. 14). The 160 and 190 keV lines were unresolved, forming a composite peak. The shape of the composite peak differed very little from that of the Gaussian as can be seen from Figs. 37 and 8. This perhaps would indicate the insensitivity of the arithmetic probability plot for such an analysis. The lines were, however, resolved by plotting the counts per channel along a logarithmic scale and the channel number along a linear scale. A true Gaussian has a parabolic shape on such a semi-log graph paper. From the composite peak two parabolas were constructed corresponding to the two superimposed peaks (Fig. 38). These two parabolas were analysed for their Gaussian shape as well as for the mid-channels for energy determinations. The resolutions of these two parabolas were consistent with their energies as is shown in Fig. 8.

The ratio of areas of the two parabolas showed the measured intensity of the 190 keV γ -ray to be about $1/4$ that of the 160 keV one. An analysis following a method developed by P. Onno confirmed the existence of two components in the composite peaks and also their energies and relative intensities. The half-lives of these two components cannot be measured

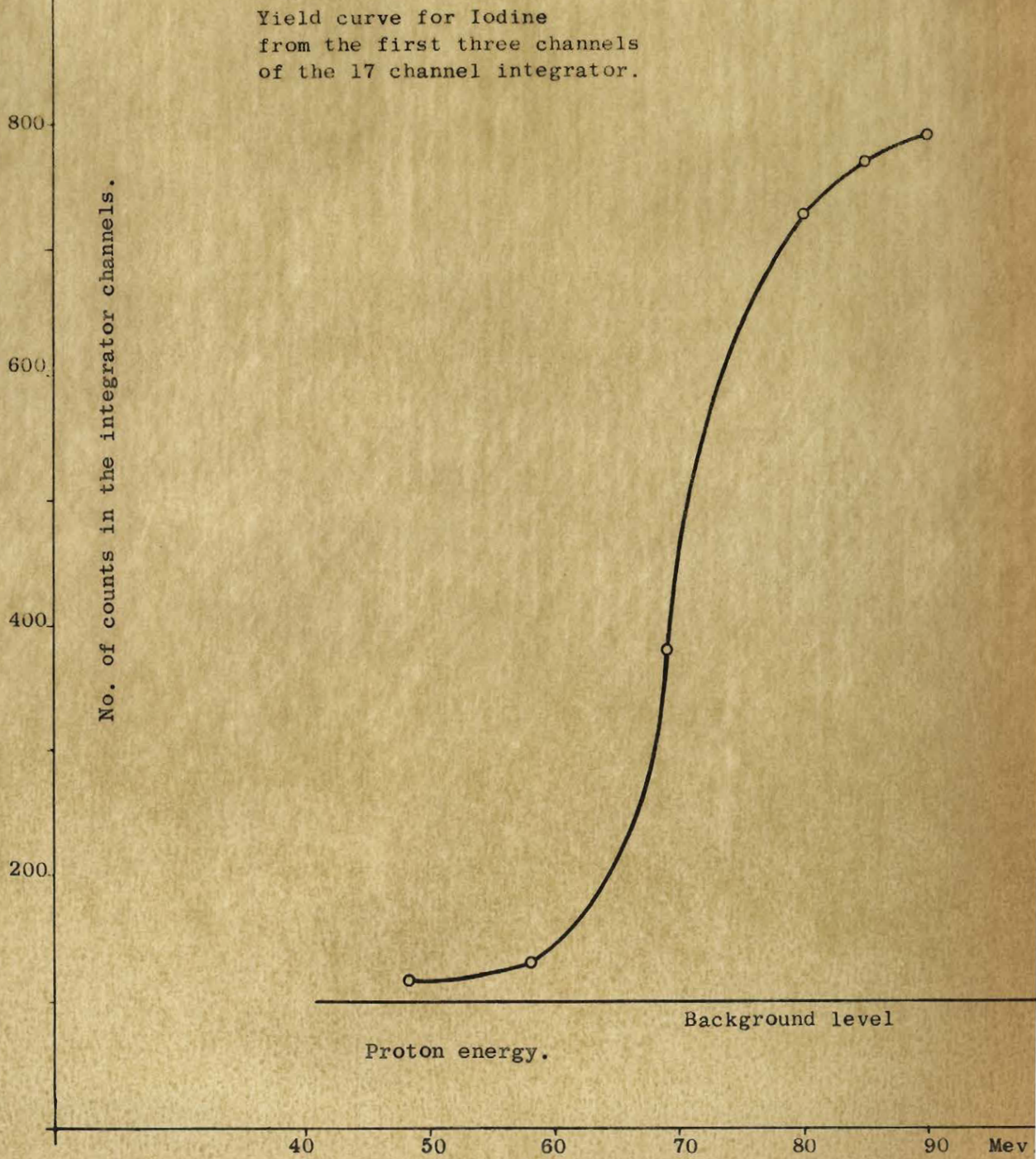
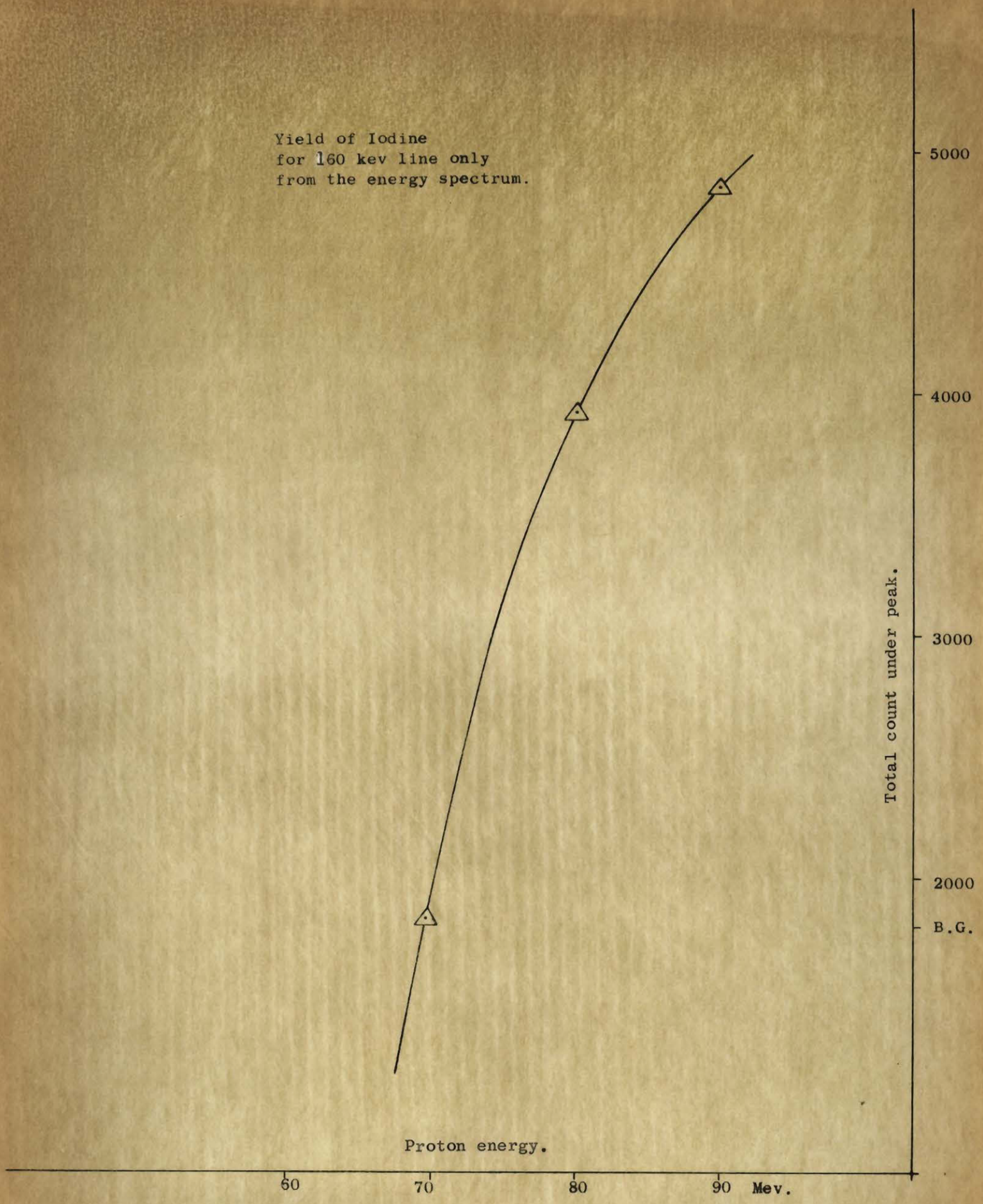


Fig. 33

Yield of Iodine
for 160 kev line only
from the energy spectrum.



Proton energy.

Total count under peak.

2000
B.G.

5000

4000

60

70

80

90

Mev.

Fig. 34

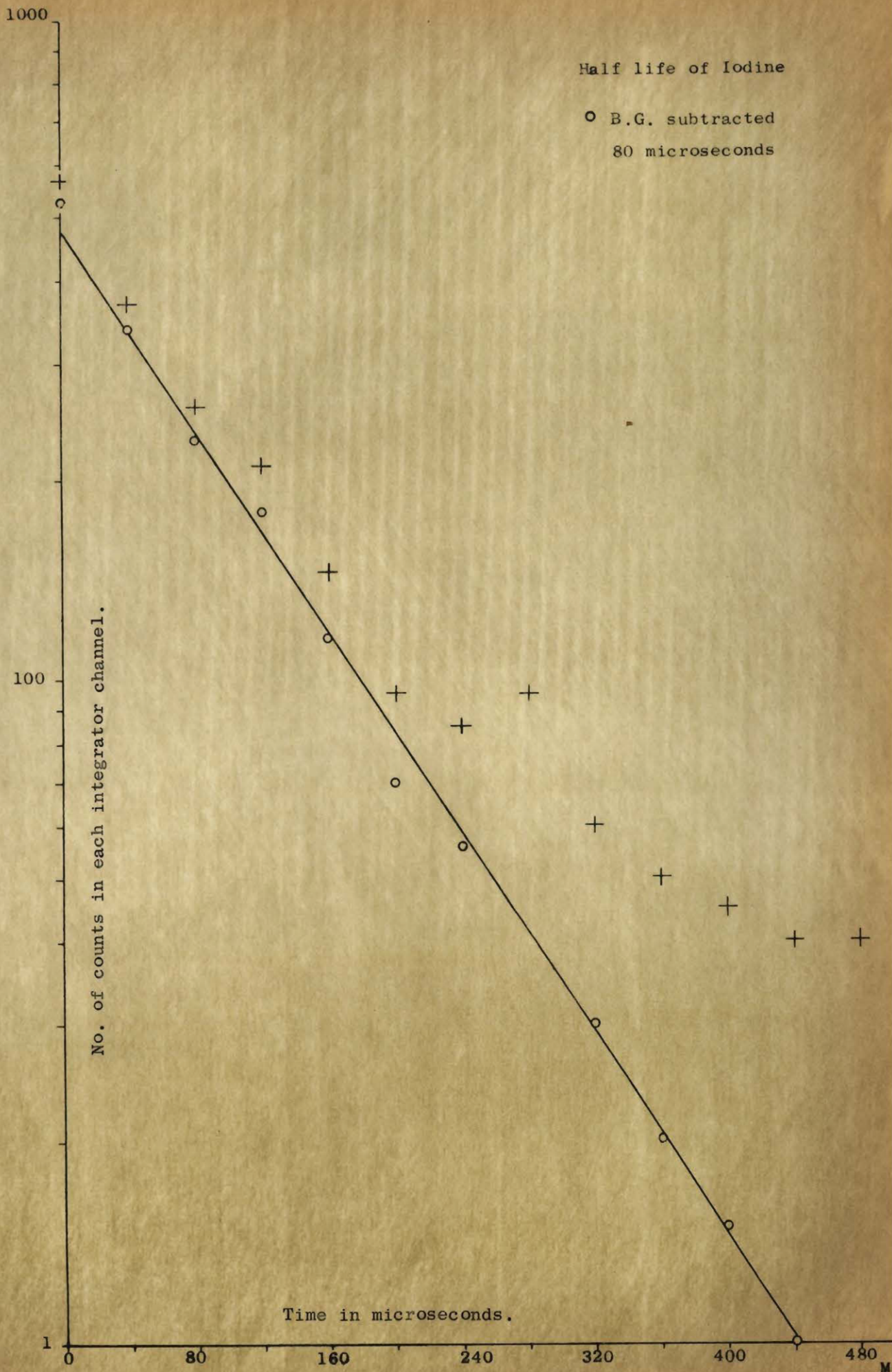


Fig. 35

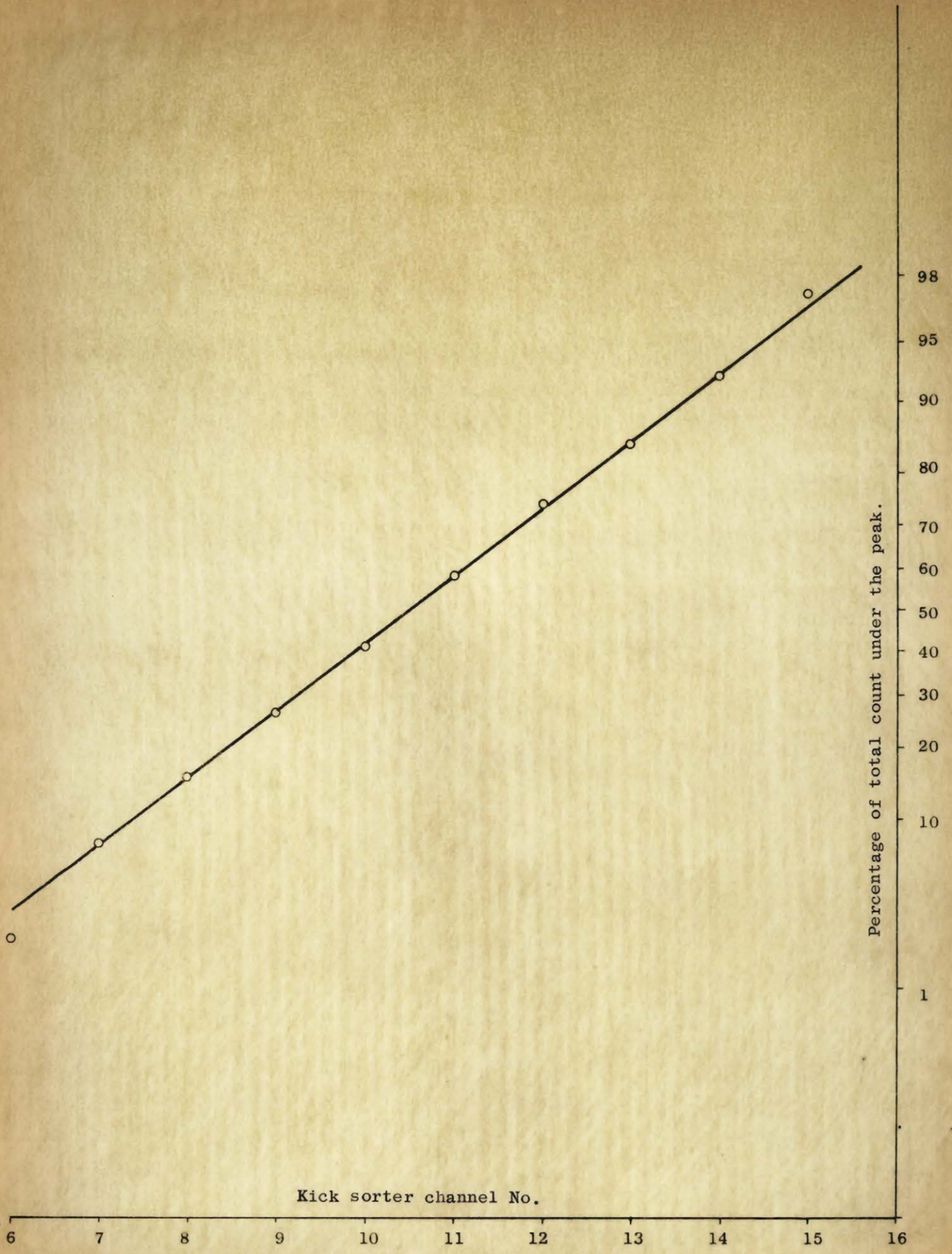


Fig. 36 Gaussian distribution of 32.88 kev calibration line.

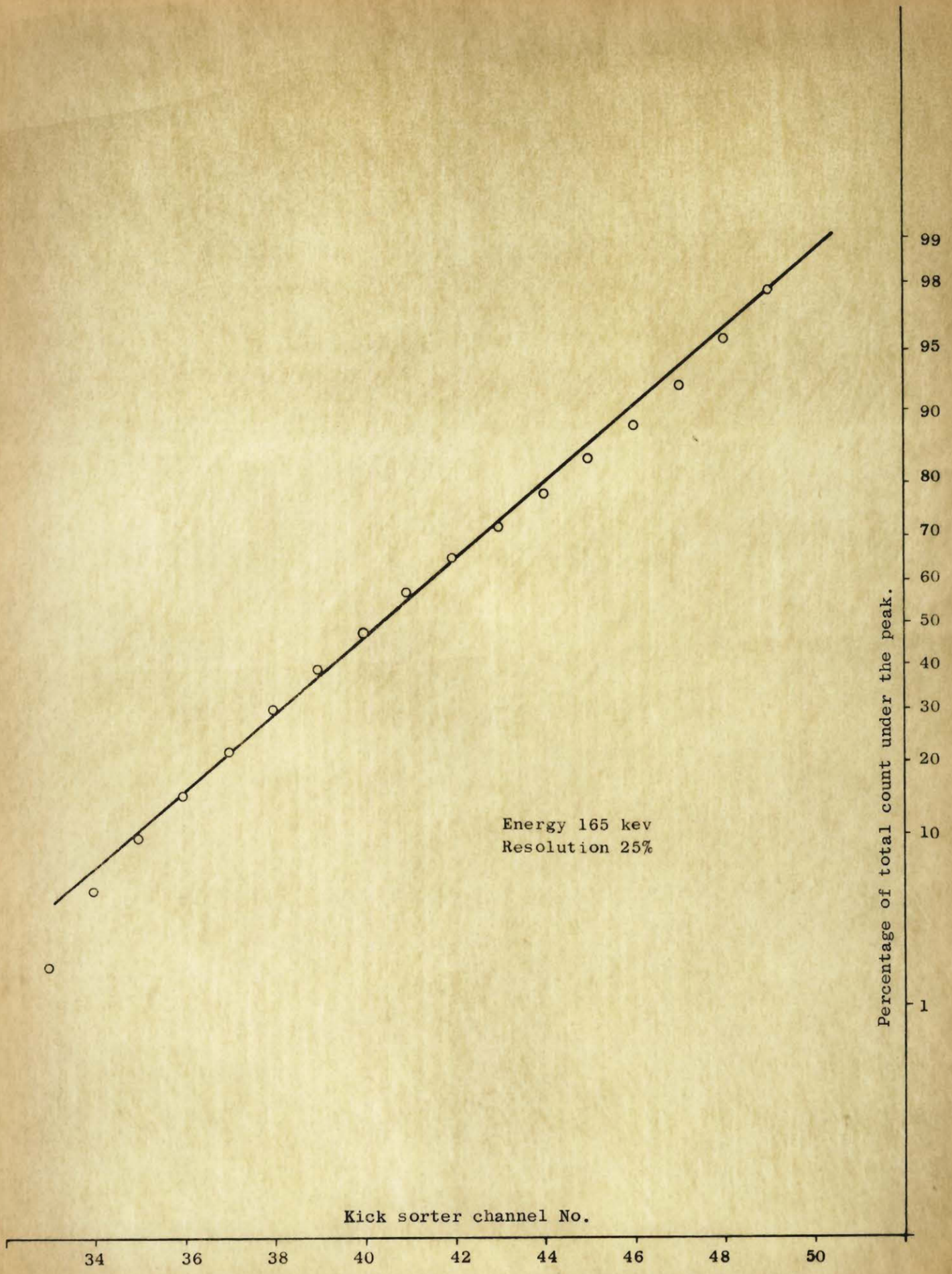


Fig. 37 Gaussian distribution of composite peak at 165 kev of Iodine.

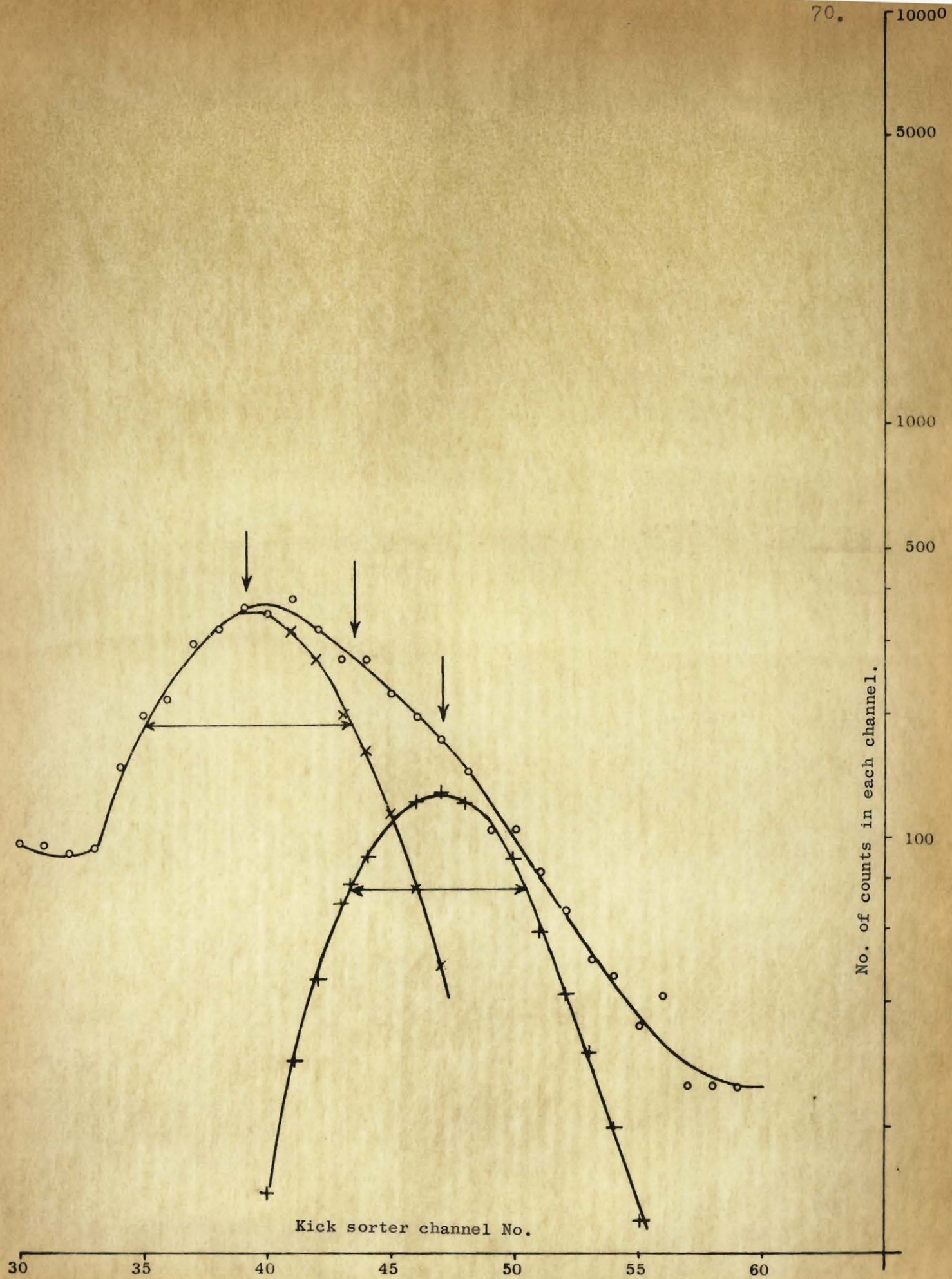


Fig.38 Analysis of the composite peak at about 165 kev. Iodine.

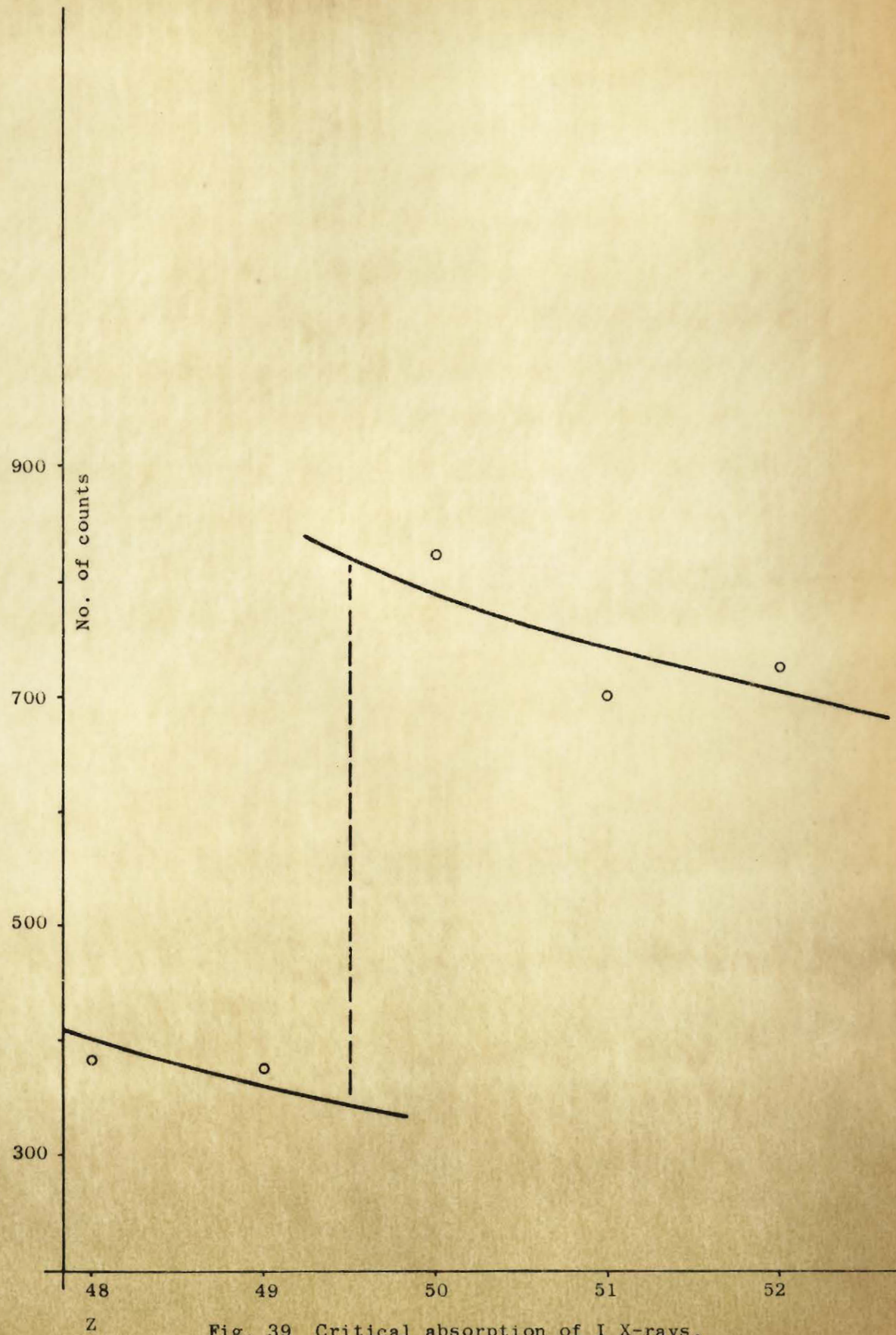


Fig. 39 Critical absorption of I X-rays.

separately. However the relative intensities did not change as a function of the first delay time. The composite peak was recorded for delays of $50 \mu s$, $100 \mu s$ and $200 \mu s$, and was analysed into two components on semi-logarithmic paper. The intensity ratio was the same in each case. The half-life of the two softer γ -rays was measured independently of the composite peak by means of the single channel bias and had the same value as that of the composite peak. Further, the relative intensities of the 60 kev and 96 kev and the composite peak were observed to remain constant when the first delay period was varied. The arithmetic probability plots of all the four lines were reasonably straight and yielded the expected values of the resolutions as can be seen from Fig. 8. The energies of the four γ -rays were obtained from the probability graphs of the peaks and that of a calibration line.

The yield curve was obtained by both the methods described elsewhere (Fig. 33 and 34). The threshold value of the yield is taken as 48 Mev.

The critical absorption of the X-rays established the Z-value of the isomer to be 53 (Fig. 39). Thus the reaction is (p, p α n) as in the case of antimony. The threshold of the reaction of 48 Mev corresponds to a mass difference of 6 neutrons. Thus the reaction suggested is $^{127}_{53}\text{I} (p, p6n)$ $^{121}_{53}\text{I}$.

The suggested decay scheme (Fig. 41 (c)) is the only one of the numerous possibilities considered which satisfies reasonably well the various requirements related to the addition of energies, the ratios of intensities, and the estimated rates of decay and which at the same time leads to assignment of spins and parities which are plausible in view of the shell model. The results of calculations related to this decay scheme are tabulated in Table IV.

The alternative possibilities can be ruled out on the following grounds.

1. A comparison of the intrinsic counts of X-rays and 160 keV γ -rays from Table IV would indicate this γ -ray to be practically unconverted and therefore necessarily of low multipolarity.
2. 60 keV cannot be an E2 transition, in which case it alone would account for the total X-rays observed. Thus the additional number of X-rays from the remaining three γ -rays would remain unaccounted for.
3. 96 and 60 keV γ -rays can be parallel only to the 160 keV lines, allowing for the limits of accuracy of measuring the energies. But this limit does not allow 96 and 60 keV to be parallel to 190 keV.
4. 190 keV γ -ray would have to have a rather high internal conversion coefficient (corresponding to multipolarities of order higher than 2) to be in cascade with 160 keV one. This requirement does not agree with the observed X-ray intensity and Weisskopf's estimates.
5. The intensity considerations would rule out the possibility of 96 and 60 keV γ -rays being parallel to the 160 keV one. This would simply increase the discrepancies outlined in 4 to a greater extent.
6. All the four cannot be in cascade on the grounds mentioned in 4 and 5 and further on the grounds of the relative intensities.

From all these it becomes clear that 190 keV and 160 keV have to be in parallel branches to fit the observed intensities. The energy discrepancy of these two can just be filled by placing the 60 keV γ -ray in cascade with the 190 keV one, with the 160 keV and 96 keV γ -rays forming the other branch.

The computed values of the X-ray intensity and the populations of the four excited states are given in Table IV. These values are consistent and in fair agreement with observed intensities given in Table IV.

The ground state of ${}_{53}^{121}\text{I}_{68}$ is reported to be a $5/2^+$ state (9).

On the basis of the suggested reaction and the decay scheme, therefore, the spin and the parity assignments of the four levels involved in this isomeric transition would be due to the single odd proton as shown in Fig. 41 (c). This would imply that in ${}_{53}^{121}\text{I}$ the $1g^{7/2}$ and $2d^{5/2}$ levels are interchanged in order (i.e. $1g$ state is higher than $2d$); further that $1h^{11/2}$ level is lowered down to a position in between the $2d^{5/2}$ and $2d^{3/2}$ levels.

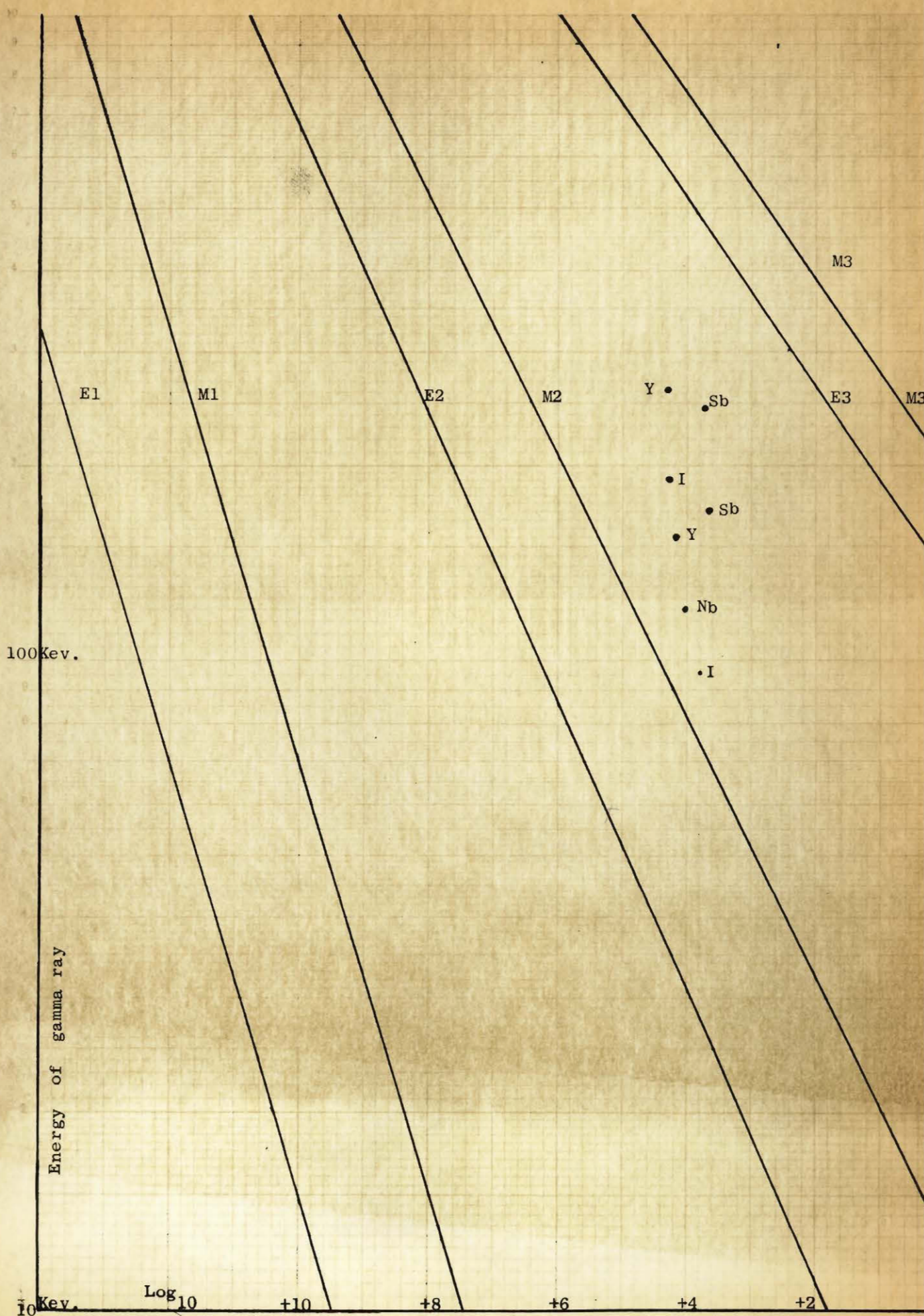


Fig. 40. Chart for Weisskopf estimates, and positions of the isomers.

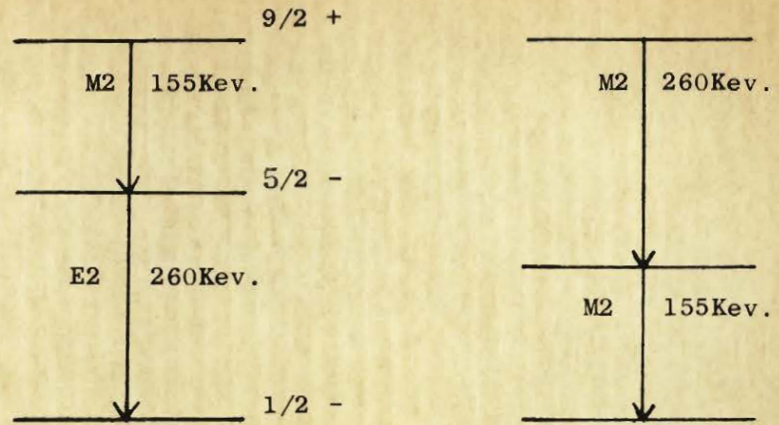


Fig. 41 a.
Decay schemes for yttrium.

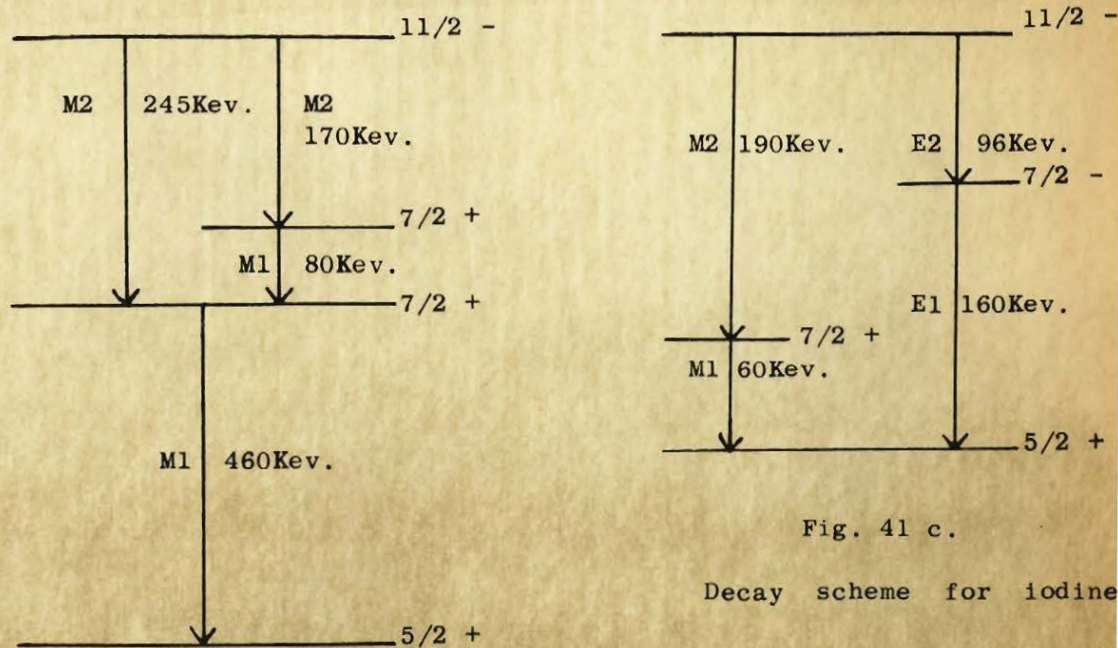


Fig. 41 b.
Decay scheme for antimony.

Fig. 41 c.
Decay scheme for iodine

Fig. 41.

Table I.

Description of calibration lines	Energy	Resolution*
1.28 Mev γ -ray from Na ²²	1.28 Mev	5%
662 kev γ -ray from Cs ¹³⁷	662 kev	10%
Annihilation radiation from Na ²²	511 kev	12%
Pt. X-rays from Au	68.4 kev	34%
Ba X-rays from Cs ¹³⁷	32.88 kev	40%

* Full width at half-maximum.

Table IIa - Yttrium

Energy	Resolution	Observed No. of counts	Counting Efficiency	Intrinsic Count	Total				log λ
					α_1	α_2	β_1	β_2	
155 kev	40%	2266	3.2×10^{-2}	7.08×10^4	.03	.29	.055	.43	4.2
260 kev	22%	1559	1.6×10^{-2}	9.74×10^4	.007	.034	.012	.07	4.3

Table IIb - Niobium

Energy	Resolution	Observed No. of counts	Counting Efficiency	Intrinsic Count	Total		Log λ
					α_2	β_2	
120 kev	27%	2400	4×10^{-2}	6×10^4	0.61	1.2	3.8

Table III (a)

Energy	Observed No. of counts	$\mu p \times \rho x$ for source	$\mu p \times \rho x$ for aluminium	Counting Efficiency	Intrinsic No.	Ratio of counts
26 kev (X-ray)	960	7.3×0.125	1.2×0.035	3.8×10^{-2}	6.57×10^4	1.825
80 kev	1100	2.7×0.125	0.18×0.035	4.3×10^{-2}	3.60×10^4	

Table III (b)

Energies	26 kev X-ray	80 kev	170 kev	245 kev	460 kev
Resolution	Corresponding	31.5%	-	-	15%
Observed No. of counts	No. of X-rays	1500	1066	1420	1700
Counting efficiency	is obtained	4.3×10^{-2}	2.75×10^{-2}	1.8×10^{-2}	7.5×10^{-3}
$\mu p \times \rho x$ for source	from: $1.825 \times$	2.7×0.38	0.42×0.38	0.21×0.38	0.10×0.38
$\mu p \times \rho x$ for aluminium	9.79×10^5	0.18×0.035	0.13×0.035	0.12×0.035	0.08×0.035
Intrinsic count	$= 1.79 \times 10^5$	9.79×10^4	8.05×10^4	8.58×10^4	2.36×10^5
	α_1	0.28	.037	.013	.0026
Int. conversion	α_2	2.1	0.21	.055	.0085
coefficients	α_3	13.0	0.98	0.22	0.023
	β_1	0.95 (1.0)	0.12	.046	0.01 (0.011)
	β_2	11.0	0.78 (0.97)	0.18 (0.26)	0.020
Suggested K-conversion		9.30×10^4	6.28×10^4	1.74×10^4	0.27×10^4
Level population "n" for suggested decay		1.9×10^5	1.58×10^5	1.08×10^5	2.39×10^5

N.B. The figures inside brackets are total int. conversion coefficients.

Table IV

	28 kev X-ray	60 kev	96 kev	160 kev	190 kev
Resolution		35.8%	30.0%	24.5%	24.5%
Obs. No. of counts	2360	500	1100	3075	800
Counting Efficiency	3.8×10^{-2}	4.2×10^{-2}	4.3×10^{-2}	3.0×10^{-2}	2.0×10^{-2}
$\mu/\rho \times \rho x$ for iodine	6.5×0.075	6.25×0.075	1.85×0.075	0.58×0.075	0.34×0.075
$\mu/\rho \times \rho x$ poly. cover	0.35×0.159	0.19×0.159	0.17×0.159	0.15×0.159	0.13×0.159
$\mu/\rho \times \rho x$ for Al.	1.40×0.035	0.25×0.035	0.16×0.035	0.13×0.035	0.12×0.035
Intrinsic Count	1.12×10^5	1.98×10^4	3.05×10^4	1.09×10^5	4.20×10^4
Int. conversion α_1		0.76	0.20	0.04 (.049)	0.02
Coefficients α_2		5.2	1.40 (2.09)	0.26	0.15
β_1		2.8 (3.23)	0.76	0.17	0.15
β_2		42.0	7.80	1.30	0.72 (0.80)
Suggested K-conversion		5.74×10^4	4.27×10^4	0.54×10^4	3.02×10^4
Level population		8.31×10^4	9.45×10^4	1.14×10^5	7.56×10^4

*N.B. The figures inside brackets are total int. conversion coefficients.

Thus total K-conversion = 1.357×10^5

Total K X-rays emitted = 1.15×10^5 (reduced by fluorescent yield)

Total X-rays observed = 1.12×10^5

No. of 60 kev M1 levels \approx No. of 190 kev M2 levels.

No. of 96 kev E2 levels \approx No. of 160 kev E1 levels.

VI. Summary.

New isomers have been found to result from the proton bombardment of yttrium, niobium, antimony and iodine. No isomeric state was detected using copper, cesium, silver, indium targets. All are odd-even isotopes. Copper, silver, indium and antimony have two isotopes, the other four are mono-isotopic.

In each of the four cases the energies of the γ -rays, the half-life and the yield curve have been measured. Attempts have been made to identify the nuclear reaction which has taken place from the shape of the yield curve. In the case of antimony and iodine, the associated X-rays have been observed as well and their critical absorption has established the atomic number of the isomeric nucleus (Fig. 32 and 39). Relative intensities of the γ -rays and X-rays where present enable one to determine the internal conversion coefficients and hence the nature and multipolarity of the transition. Furthermore, the corrected values of the transition probabilities are compared with the Weisskopf estimates in the light of data on existing nuclear isomers (7). Where it has been possible to assign the isomeric state to a specific nucleus and to propose a decay scheme, correlation with shell theory has been attempted.

VII. Acknowledgements.

It is a pleasant duty to acknowledge gratefully the support and interest of Dr. J. S. Foster to carry out the present investigation. Thanks are also due to Dr. R. E. Bell, the present Director of the Radiation Laboratory, for his continued support and interest.

The present thesis owes its origin largely to the guidance and advice of Dr. W. M. Martin, the research Director. The author is grateful (to him) for his valuable time and assistance during every phase of this investigation.

The advice and assistance of Dr. A. L. Thompson in procuring, testing and preparing the targets and the X-ray absorbers, are acknowledged with thanks. The suggestions and help of Mr. C. K. Hargrove are thankfully acknowledged. The co-operation of Mr. R. H. Mills and Mr. C. Weissfloch in operating the cyclotron, and of Mr. S. Doig and staff of the machine shop are acknowledged with thanks.

The assistance of Mr. D. Robertson in numerical computations and graphical compilations and of Mrs. D. Neilson in typing the thesis in its various stages deserves special thanks and acknowledgement.

VIII. Bibliography.

- (1) Cross, W. G., 1951. R.S.I. 22:717.
- (2) Hunt, J., Ph.D. Thesis (Physics) McGill University.
- (3) Hargrove, C.K., Ph.D. Thesis (Physics) McGill University, 1961.
- (4) Link, W. T., Ph.D. Thesis (Physics) McGill University, 1957.
- (5) Skarsgard, H. M., Ph.D. Thesis (Physics) McGill University, 1955.
- (6) Wapstra et al. Nuclear Spectroscopic Tables. North-Holland Pub. Co., Amsterdam.
- (7) Goldhaber, M. and Sunyar, A. W. Beta- and gamma-ray spectroscopy. Edited by K. Siegbahn. North-Holland Pub. Co., Amsterdam.
- (8) Bell, R. E. Proceedings of an informal conference. Gatlingburg, Tennessee, Sept. 1956. Publication No. 467. National Academy of Sciences, National Research Council.
- (9) Goldhaber, M. and Hill, R. D. 1952. Rev. Mod. Phys., 24:179.
- (10) Metropolis and Reitwiesner. Table of Atomic Masses.
- (11) Halsted, R.E., 1952. Phys. Rev. 88:666.
- (12) Mayer, M. G., 1949. Phys. Rev. 75:1969.
- (13) Rose, M. E. Tables of internal conversion coefficients. North-Holland Pub. Co., Amsterdam.
- (14) Haxel, O., Jensen, J.H.D. and Suess, H.E. 1949, Phys. Rev. 75:1766.
- (15) Goldhaber, M. 1950. Phys. Rev. 79:193.
- (16) Forsling, W. and Ghosh, A., 1952. Arkiv For Fysik, 4:331.